wisconsin astrophysics

August 1981

Number 137

EXTENDED ADIABATIC BLAST WAVES

AND

A MODEL OF THE SOFT X-RAY BACKGROUND

Donald P. Cox and Paul R. Anderson

Space Physics Laboratory, Department of Physics, University of Wisconsin

ABSTRACT

An analytical approximation is generated which follows the development of an adiabatic spherical blast wave in a homogeneous ambient medium of finite pressure. At early times, when the external pressure is negligible, the structure is that of the usual self-similar solution. At later times, the structure evolves smoothly as the shock weakens, the post-shock compression declines, and the gradients in pressure and density become less severe within the shocked region. The complete structure should be reliable down to a post-shock compression of about 2, with conditions close inside the shock remaining well-described somewhat longer.

An analytical approximation is also presented for the electron-temperature distribution resulting from coulomb collisional heating. It is shown that thermal conduction, limited by saturation at early times, fades in importance just as coulomb-collisional heating becomes significant. An estimate is made of the nonequilibrium cooling coefficient and the degree of ionization equilibration expected by the time significant cooling sets in. From this, estimates of the endpoint of the adiabatic era, based on the collisional equilibrium emissivity, are shown to be reasonably accurate.

The dynamical, thermal, ionization, and spectral structures are calculated for blast waves of energy $E_0 = 5 \times 10^{50}$ ergs in a hot low-density interstellar environment. A formula is presented for estimating the luminosity evolution of such explosions, including the effects of nonequilibrium ionization. It is then shown that the B and C

bands of the soft X-ray background are reproduced by such a model explosion if the ambient density is about 0.004 cm^{-3}, the blast radius is roughly 100 pc, and the solar system is located inside the shocked region. The age of such an explosion is roughly 10^5 years. This result is almost independent of whether there is appreciable noncoulomb heating of the electrons. The M band count rate for the model is considerably less than what is observed, consistent with the suggestion that this radiation is independently produced, possibly in the galactic corona or beyond.

Two regions of the sky, however, which have enhanced X-ray emission, and which may be such explosion-heated bubbles viewed from outside, are both, like the background, brighter than the models in the M band. The OVI column density measurements also provide difficulties: models with a homogeneous ambient medium seem to require an ambient (preshock) temperature greater than 3×10^5 K if the medium extends only slightly beyond the shocked region, or greater than 8×10^5 K if it fills a substantial portion of the interstellar volume. It is suggested that evolution in a pre-existing cavity with a strong density gradient may remove both the M band and OVI discrepancies.

Subject headings: interstellar: matter - shock waves - X-rays: general

Introduction

This paper consists of four sections merging material from two separable but related investigations. In the first section, an analytic approximation is presented for the nonsimilar time evolution of the dynamical structure of an adiabatic blast wave generated by a point explosion of energy E_0 in a homogeneous ambient medium of density ρ_0 and pressure p_0. At early times, this solution resembles the zero pressure similarity solution of Taylor (1950) and Sedov (1959), but extends the range of investigation well into the regime in which the external pressure is significant.

In the second section, the thermal history of the material is discussed. In particular, a scheme is presented for evaluating the electron temperature distribution for the evolving structure of §I if only coulomb collisions between electrons and ions serve to heat the electrons. Approximations to the distribution at early times are also given in order to provide a good description of the rate at which the equilibration between electron and ion temperatures takes place.

The estimate of the cooling time of a blast wave is reviewed. Such estimates, however, are based on the assumptions that the electron and ion temperatures have equilibrated and that the ionization states are in collisional equilibrium with that temperature. The first of these is shown to be valid before significant cooling occurs, but the second is less easily tested. Hence an estimate of the cooling coefficient is made for the assumption that the ionization level is lower than in collisional equilibrium, and it is shown that the cooling rate, although generally

higher than in equilibrium, approaches the equilibrium rate before significant cooling takes place, verifying the approximate validity of cooling time estimates based on the above assumptions. This is then rechecked by estimating the degree of ionization equilibration versus time, evaluating the results at the cooling epoch.

In the third section, a procedure is presented for following the state of a given fluid element through the evolving dynamical and thermal structures of §I and §II, and a computer program is described which then calculates the ionization state, emissivity, spectrum, luminosity, etc. for such a blast wave. The luminosity evolution for a set of diagnostic runs is presented and compared with estimates based on §II. In addition, for two runs, the dynamical, thermal, and oxygen ionization structure are presented, as are the surface brightness spectra.

In the fourth section, the models generated are applied to a discussion of the soft X-ray background. It is hypothesized that this background radiation derives in part from the thermal emission of a very large blast wave within which the solar system is immersed. Using equilibrium models and clues from the properties of the background as a guide, the required blast wave is estimated to have a radius of about 100 pc, a characteristic temperature of about 10^6 K, and to be propagating into an ambient density of about 0.004 cm^{-3}. The required energy is about 3×10^{50} ergs, coincidentally similar to the energy released by a supernova explosion.

The diagnostic runs of section §III had been chosen to test this hypothesis. Thus the resulting surface brightness spectra are translated into the band count rates which would be observed by the Wisconsin soft

X-ray astronomy group's rocket payload. These are then compared with the observed count rates, with the result that the two lowest band rates can easily be produced, but the medium-energy band apparently cannot. Two possible remedies for this deficiency are discussed.

The OVI column densities calculated for these runs are then interpreted and compared with an upper limit imposed by observations. It is found that, in general, there is too much O^{+5} and several ways to avoid this are discussed.

Finally, in §V, the conclusions pertinent to the application in §IV are presented.

Readers interested primarily in fluid mechanics should concentrate on §I where the extrapolation of an approximation scheme due to Kahn (1975) has provided considerable insight into a problem without exact analytical solution. Those whose interest focuses on the evolution of normal supernova remmants should skim §II with particular attention to IID. Those who care most about the soft X-ray background, the local interstellar medium, or the possibility of a galactic corona could begin with §IV.

I. The Dynamical Evolution of An Adiabatic Blast Wave into a Region of Finite Pressure

A. Equations of Motion and Normalized Variables

The evolution of an explosion of energy E_0 into a cold (zero pressure) homogeneous medium of density ρ_0 is described by the similarity solution of Sedov (1959). The evolution of a similar explosion into a

region of non-negligible ambient pressure, p_0, has been approximated by Gaffet (1978). Kahn (1975) has given a method for generating simple high quality analytic approximations to the Sedov structure; we here generalize this method to give comparable results for the $p_0 \neq 0$ case.

The equations of mass, energy, and momentum conservation in a spherically symmetric adiabatic gas with $\gamma = 5/3$ are, respectively,

$$\frac{\partial \rho}{\partial t} = -\frac{1}{R^2}\frac{\partial}{\partial R}(R^2 \rho u), \quad \frac{D}{Dt}(p/\rho^{5/3}) = 0, \quad \frac{Du}{Dt} = \frac{\partial u}{\partial t} + u\frac{\partial u}{\partial R} = -\frac{1}{\rho}\frac{\partial p}{\partial R} \qquad (1)$$

where R is the distance from the explosion site, $u = DR/Dt$ is the velocity of a parcel of gas at R, and ρ, p are density and pressure.

The region of the shock disturbed material is bounded by the shock radius, R_s, expanding outwardly with velocity v_s. The jump conditions relating conditions just inside the shock to those outside are

$$v_s^2 = \frac{5}{3}\frac{p_0}{\rho_0} + \frac{4}{3}\frac{p_0}{\rho_0}(y_s - 1), \quad x_s = \frac{4y_s + 1}{y_s + 4}, \quad u_s = \left(\frac{x_s - 1}{x_s}\right) v_s \qquad (2)$$

where the normalized variables $x = \rho/\rho_0$, and $y = p/p_0$ have been introduced and the subscript s refers to post-shock conditions. Three further normalized variables will also be of use:

$$r = R/R_s, \quad \kappa = y/(x)^{5/3}, \quad \mu = M(R)/M(R_s) = \int_0^r 3r^2 x\, dr \qquad (3)$$

where $M(R_s) = 4\pi R^3 \rho_0 /3$ and κ is the adiabatic invariant for a parcel of gas.

B. Boundary Conditions at $r \sim 0$ and $r \sim 1$

Early in the evolution of the explosion, the Sedov solution will be appropriate, in which case

$$R_s = \left(\frac{2.02\, E_o}{\rho_o} t^2 \right)^{1/5}$$

$$v_s = \frac{dR_s}{dt} = \frac{2}{5} \frac{R_s}{t}$$

$$p_s = \frac{3}{4} \rho_o v_s^2 = \frac{3}{25} (2.02\, E_o)/R_s^3 \qquad (4)$$

$$x_s = 4$$

$$\kappa_s = y_s/x_s^{5/3} = \frac{6.06}{25(4)^{5/3}} \frac{E_o}{\rho_o R_s^3} = \frac{6.06\, \pi}{75(4)^{2/3}} \frac{\rho_o E_o}{\rho_o M_s} .$$

As the evolution proceeds, material shocked early enough to be governed by the Sedov equations will be left behind by the shock front, eventually becoming part of the central region. In this region the sound speed remains quite high (if the adiabaticity assumption remains valid) and the pressure is nearly uniform. During the flow, any given shell of this interior material retains two constants of the motion, the mass enclosed by the shell and the adiabatic invariant, κ, the latter being determined by equation (4). From the dependence of these two constants on one another, the central density structure can be inferred as a function of position and the value, y_I, of the normalized pressure in the central plateau. The results can best be expressed in terms of a characteristic radius defined by

$$R_c^3 \equiv \frac{2.02\, E_o}{75\, p_o} \qquad (5)$$

at which the effects of the external pressure begin to be felt. (This

particular choice simplifies equation(11).)

The resulting central density distribution is

$$x = 4(\frac{8}{25})^{3/2}\, y_I^{\,3/2}\, (\frac{R}{R_c})^{9/2} = 0.30\, y_I^{\,3/2}\, (\frac{R}{R_c})^{9/2} \qquad (6)$$

The particular result from this discussion which is useful in applying Kahn's method to the structure is that, so long as there is a central pressure plateau, μ is proportional to $r^{15/2}$ making

$$\frac{1}{\mu}\frac{\partial \mu}{\partial r} \simeq \frac{15}{2r} \qquad \text{(central regions)}. \qquad (7)$$

Just behind the shock front, the derivatives of pressure, density, gas velocity, and μ can be found by combining the equations of motion (1) and the jump conditions (2). However, they also depend on the deceleration rate of the shock front itself. This deceleration rate can be expressed in terms of the parameter

$$\alpha \equiv R_s\, dy_s/dR_s \qquad (8)$$

since knowing $\alpha(R_s)$ is equivalent, through the jump conditions, to knowing $v_s(R_s)$, and therefore $R_s(t)$ by normalizing to the Sedov solution which is appropriate for $R_s \ll R_c$. In this limit, $R_s^{\,3} y_s \to 9R_c^{\,3}$ and $\alpha \to -3y_s$.

The resulting derivatives evaluated at $r = 1$ are:

$$\frac{1}{y}\frac{\partial y}{\partial r} = -\frac{5}{2} - \alpha\left[\frac{5}{2(y_s-1)} + \frac{y_s-1}{y_s(y_s+4)}\right]$$

$$\frac{1}{x}\frac{\partial x}{\partial r} = -\frac{3}{2} - \alpha\left[\frac{3}{2(y_s-1)} + \frac{3(y_s-1)}{(y_s+4)^2}\right]$$

$$\frac{1}{u} \cdot \frac{\partial u}{\partial r} = -\frac{5}{2}\frac{y_s}{y_s-1} - \frac{\alpha}{2}\frac{(3y_s+2)}{(y_s-1)^2} \qquad (9)$$

$$\frac{1}{\mu}\frac{\partial \mu}{\partial r} = 3x_s$$

$$\frac{\partial^2 \mu}{\partial r^2} = \frac{\partial}{\partial r}(3r^2 x) = 3\,x_s\left[2 + \frac{1}{x}\frac{\partial x}{\partial r}\right].$$

Abbreviating the partial derivatives with primes, the derivatives at early times (when $y_s \gg 1$, $x_s = 4$, $\alpha = -3y_s$) are $y' = 8y_s$, $x' = 48$, $u' = 2u_s$, $\mu' = 12$, $\mu'' = 168$.

C. The Evolving Shock Strength

In order to proceed further, a reliable approximation is needed for $\alpha(R_s)$, or $\alpha(y_s)$. We suggest that

$$\alpha = -(y_s-1)\,(3-2/y_s) \qquad (10)$$

has several desirable properties. First, it approaches $-3y_s$ at large y_s, as required by the Sedov solution. Secondly, it degenerates to $-(y_s-1)$ as $y_s \to 1$, appropriate to a spherically symmetric sound wave with amplitude inversely proportional to R_s (i.e. $R_s(y_s-1)$ approaches a constant). Thirdly, at $y_s=6$, it has the value $-40/3$. At $y_s=6$, $x_s=2.5$, and with this value of α, $d(\ln x)/d(\ln r) = 9/2$ at $x=1$ as well as at $x=0$. The density distribution then has the simple form $x=2.5\ r^{9/2}$ at this epoch. Thus the density distribution in a log-log plot passes smoothly through a single power law as it changes from concave upward at early times to concave downward at late times.

Finally, since this approximation to α determines the time evolution of R_s, and underlies much of the remaining discussion of this paper, Eric Jones of

Los Alamos was asked to run a purely adiabatic, numerical-hydrodynamical calculation of an explosion into a medium of finite pressure.. He did so (Jones, 1978), following the explosion to $y_s = 2$. Because of the finite cell size in the numerical calculation, neither the shock position nor post shock pressure is known exactly. Within the uncertainties, however, there is essentially perfect agreement between his results and the integrated form of equation (10):

$$\frac{R_s^3(y_s-1)^3}{(3y_s-2)^2} = \text{constant} = \frac{2.02\ E_o}{75\ p_o} = R_c^3 \qquad (11)$$

giving the evolution of the post-shock pressure with R_s, normalized to the Sedov solution at early times.

D. The Evolving Dynamical Structure

1. The Kahn Method and its Extension

Kahn (1975) suggested that since $(1/\mu)(\partial\mu/\partial r) \to 15/2r$ as $r \to 0$ and $\partial\mu/\partial r = 3x_s$ at $r = 1$ where $\mu = 1$, the general mass distribution might be fairly well described by the form

$$(1/\mu)(\partial\mu/\partial r) = 15/2r + (3x_s - 15/2)\ r^{\beta} \qquad (12)$$

where the unknown β is found by forcing $\mu'' = 3x_s[2 + x'/x_s]$ at $r = 1$ as required by equation (9).

This procedure automatically gives the correct density distribution near the edge. Use of the adiabaticity then assures the correct pressure distribution there. So long as $\beta > -1$, it also gives the correct slope

for ln ρ near the center, although the density normalization is not guaranteed. In fact, however, the procedure seems to give a quite accurate description for a blast wave into negligible pressure. (See Cox and Franco, 1981, for a comparison.)

We now attempt this procedure for the non-negligible p_o case. Differentiation of equation (12) yields (at r = 1)

$$\mu'' = -15/2 + ((3x_s - 15/2)\beta + (3x_s)^2 \qquad (13)$$

Setting this equal to $3x_s[2 + x'/x_s]$ at r = 1 with x'/x_s from equation (9), α in that equation from equation (10), and eliminating y_s in favor of x_s using equation (2), β can be evaluated. A more convenient parameter for later work is q = β + 1 and the result is

$$q = \beta + 1 = \frac{2}{3}\ \frac{x_s(x_s-1)(7x_s-13)}{(4x_s-1)} \qquad (14)$$

Equation (12) can be integrated to find the mass distribution

$$\mu(r) = r^{15/2} \exp\left[\left(\frac{3x_s - 15/2}{q}\right)(r^q - 1)\right] \qquad (15)$$

from which the density distribution can be found, using $\mu' = 3r^2x$ from equation (3). The result is:

$$x(r) = \left[\frac{5}{2} + \left(x_s - \frac{5}{2}\right) r^q\right] r^{9/2} \exp\left[\left(\frac{3x_s-15/2}{q}\right)(r^q-1)\right] \qquad (16)$$

(where $q = q(x_s)$ from equation (14)). Similarily, the original location, R_i, of a mass element now found at $R = R_s r$ is

$$R_i = R_s[\mu(r)]^{1/3} \equiv R_s r_i \qquad (17)$$

since $\mu = (R_i/R_s)^3$ from the initially uniform density distribution.

The pressure in this parcel just after it was initially shocked follows from combining equation (11) and (17) and solving the resulting cubic equation for $y_{si}(\mu, y_s)$ to give

$$y_{si} = 1 + \frac{3}{Q} + \left\{\left(\frac{3}{Q}\right)^3 + \left(\frac{3}{Q}\right)^2 + \frac{1}{2Q} + \frac{1}{2Q}\left(1 + \frac{4}{Q}\right)^{1/2}\right\}^{1/3}$$

$$+ \left\{\left(\frac{3}{Q}\right)^3 + \left(\frac{3}{Q}\right)^2 + \frac{1}{2Q} - \frac{1}{2Q}\left(1 + \frac{4}{Q}\right)^{1/2}\right\}^{1/3} \qquad (18)$$

where $Q(\mu, y_s) = \mu(r)\ (3y_s-2)^2/(y_s-1)^3$ and y_s characterizes the present epoch. The density of the parcel just after being shocked was

$$x_{si} = \frac{4y_{si} + 1}{4 + y_{si}} \qquad (19)$$

from equation (2). The adiabaticity of the flow can now be used to find the present pressure and temperature in the parcel:

$$y = y_{si}\left(\frac{x(r)}{x_{si}}\right)^{5/3}$$

$$T = T_o\ [y(r)/x(r)] \qquad (20)$$

where y_{si} and x_{si} are both functions of r, and T_o is the ambient external temperature. The entire structure is thus obtained analytically. An example is presented in §III.

A difficulty arises, however, when one wishes to follow a collection of gas parcels in time to obtain their ionization structure. This involves inverting equation (15) to find the present location of a chosen mass point. Our procedure for doing this is described in §IIIA.

The time, $t(R_s)$, is found by integrating the differential equation between v_s and R_s. This equation results from eliminating y_s from equation (11) in favor of v_s, using equation (2), to yield

$$z \equiv \frac{R_s}{R_c} = \frac{4^{1/3}}{5} \frac{(15M_s^2 - 11)^{2/3}}{(M_s^2 - 1)} \tag{21}$$

where $M_s = v_s/c_o$ and c_o is the ambient adiabatic sound speed. This equation was approximately inverted by curve fitting (to an accuracy of better than 0.1% for $M_s \geq 2$) whereupon

$$\frac{1}{M_s} \approx \frac{z^{3/2}}{2.68} - 0.0933\, z^5 e^{-z} \tag{22}$$

was the result. At $M_s = 1.5$, $z = 2.039$, the fit gives $M_s \approx 1.519$. At $M_s = 1.25$, $z = 3.030$, it gives $M_s \approx 1.224$ so that reasonable accuracy is maintained even to $R_s \sim 3R_c$. The time is therefore

$$\begin{aligned} t(R_s) &= \frac{R_c}{c_o} \int_0^z \frac{dz}{M_s(z)} \approx \frac{R_c}{c_o} \int_0^z \left[\frac{z^{3/2}}{2.68} - 0.0933\, z^5\, e^{-z}\right] dz \\ &\approx \frac{R_c}{c_o} \left[\frac{2}{5} \frac{z^{5/2}}{2.68} - 0.0933\, J(z)\right] \end{aligned} \tag{23}$$

where

$$J(z) = 120 - (z^5 + 5z^4 + 20z^3 + 60z^2 + 120z + 120)\, e^{-z}, \tag{24}$$

completing our approximate but analytical description of the dynamical variables.

The general character and quality of the results are summarized by:

1) $y_s \gg 1$. The solutions approach Kahn's very accurate approximation to the Sedov solution.

2) y_s decreasing toward 6. The structure is well behaved and becoming less severe. The central pressure plateau is becoming flatter.

3) $y_s = 6$, $x_s = 2.5$, $R_s/R_c = 1.27$, $T_s/T_o = 2.4$, $q = 1.25$. At this epoch, $\mu = r^{15/2}$, $x = 2.5\, r^{9/2}$, and the central pressure distribution is extremely flat with $y_I \simeq 2.01$.

4) $6 > y_s > 3$. The approximation begins to have difficulties near $r = o$, where a presumably non-physical rise appears in the pressure. The description should remain reliable, however, for the vast majority of the material.

5) $y_s = 3$, $x_s = 1.857$, $R_s/R_c = 1.83$, $T_s/T_o = 1.615$, $q = 0$. At this epoch, $\mu = r^{39/7}$, $x = (13/7)r^{18/7}$, $y \to 0.41/r^{9/7}$ as $r \to o$. At this point the central pressure rise has diverged to the form given. This behavior arises from the inability of the Kahn approximation scheme to follow a density distribution which is intrinsically concave downward in a log-log plot. Even at this epoch, however, 94 per cent of the mass is exterior to the pressure minimum at $r \simeq 0.6$. In addition, that minimum has $y \simeq 1.0$, making this the earliest epoch at which the internal pressure is anywhere below the external pressure. This is confirmed in Jones' (1978) numerical results. Furthermore, detailed comparison shows that the structure remains well-described outward from about $r = 0.75$.

6) $y_s = 2$, $x_s = 1.5$, $R_s/R_c = 2.52$. This is the latest epoch at which the post shock pressure evolution of equation (11) was tested and therefore may be the latest epoch at which the post shock derivatives are reliable. At least until this point, the outermost structure should be reasonably reliable. The time evolution of equation (23) remains satisfactory to this epoch as well.

In his approach to this problem Gaffet (1978) also used the mass coordinates to follow the adiabatic material, and derived results equivalent to equation (9) relating shock strength, deceleration, and post shock derivatives.

Similarly he incorporated a deceleration rate equivalent to $\alpha = -40/3$ at $y_s = 6$. The greatest intrinsic difference in his method is that he assumed that $dy/d\mu$ was approximately constant rather than $d\ell n\ \mu\ /\ d\ell n\ r$ being given by a sum of two power laws as in the Kahn method. His approach has the inherent disadvantage that the results could not be expressed analytically.

By graphing y versus μ for a broad range of epochs from the results of this paper, we find that $dy/d\mu$ is in fact approximately constant for the outer 95% of the mass, but that the average slope can differ by several percent from the immediate post shock value determined by the acceleration parameter. This should lead to modest discrepancies between the two approximations, but these could be made to vanish in Gaffet's higher order approximation which allowed quadratic terms in $dy/d\mu$.

A second intrinsic difference, however, is the method by which the shock deceleration parameter was deduced. In our work, $\alpha(y_s)$ was deduced ab initio from plausibility arguments and checked by a numerical hydrodynamic calculation. In Gaffet's simplest approximation, he seems to have been led by energy arguments to a deceleration equivalent to $\alpha = -3y_s + 14/3$, making $(y_s - 14/9)\ R_s^3$ a constant. This is very similar to our result for $y_s \geq 6$, but clearly incorrect at large radii. Since Gaffet presents the post shock temperature and density structure evolution graphically for epochs as late as $y_s = 14/9$, an improved deceleration must have been incorporated. The way in which this was done, however, is unclear to us.

When our results are graphed in forms comparable to Gaffet's Figs. 2 and 3, we find that our density structures are essentially identical as expected for those epochs with $y_s > 6$. For lower values of y_s there is total disagreement. At small radii, our results are becoming inappropriate as described above,

whereas Gaffet's approach does not suffer quite the same fault. At large radii, we would expect continued agreement if the same deceleration rate were used. The most extreme example presented has $T_s/T_o = 1.2$, $y_s = 1.56$. Our post shock density slope is approximately twice that of Gaffet. Ours corresponds to $\alpha = -0.96$, his to $\alpha = -0.76$. These two do not correspond to the same shock radius since ours exhibits greater deceleration, so that the two density distributions at the same shock radius would be less different, but would have different shock strengths. In short, whatever method Gaffet used to find the deceleration rate did not quite agree with ours at late times.

Our results for v_s versus R_s (Fig. 2 in Gaffet) are also in disagreement. The biggest part of this discrepancy derives from the fact that Gaffet normalized his results to only a rough approximation to the Sedov solution at early times, making the slopes of both his lines in his Figure 2 about 9% low.

Finally we would like to point out that neither method should be considered seriously for a description at late times. As early as $y_s = 6$, a ripple can be seen developing in the temperature structure. At very late times, this ripple near the edge should be found in temperature, pressure, and density. As it propagates outward, it leaves behind a hot cavity (described below) within which the pressure is nearly uniform. Neither method is capable of adopting this form.

2. The Theoretical End Result

If the blast wave remained adiabatic indefinitely, the conditions in the vicinity of the explosion site long after the occurrence can be found. The procedure is similar to that used to find equation (6). One need only assume that the distribution of adiabatic constant, κ, versus enclosed mass, as implied by equation (11), is preserved as the system returns to the original

ambient pressure. The result of this calculation is shown as x_f (R/R_c) in Figure 1. The figure also shows the amount of mass which the blast wave removed from the volume bounded by R/R_c.

From the figure, the net result of the explosion is seen to be the generation of a hot ($T_f = T_o/x_f$) cavity with a steep density profile, leveling off around $R \sim 2R_c$. About 90 percent of the mass initially with $R < R_c$ has been expelled. The amount of expelled mass continues to rise, however, reaching about 2.5 M_c (where $M_c = 4\pi\rho_o R_c^3/3$) by $R = 2.5\ R_c$, the latest that equation (11) has been tested. This continued rise of the expelled mass would be incorrect if the system did not return identically to the original pressure in a finite time.

II. The Thermal Evolution

A. Electron Heating and Thermal Conduction

A long-standing uncertainty in the application of blast wave theory to supernova remnants is whether the electrons can be expected to have the same temperature as the ions (see McKee and Hollenbach, 1980). If only coulomb collisions act to equalize these temperatures, then the electrons are much colder than the ions just inside the shock front, and require a considerable length of time to heat up. Several authors (e.g., Itoh, 1978) have shown that considering the remnant as a whole, the electrons would reach equilibirum with the ion temperature over an appreciable fraction of the interior mass only after a time

$$t_{eq} = 5000 \text{ yr } E_{51}^{3/14} / n_o^{4/7} \qquad (25)$$

where E_{51} is the blast energy in units of 10^{51} ergs. Alternatively various plasma instabilities may cause the electrons to equilibrate, at least partially, with the ions in the shock front. We have no immediate preference for one of these two ideas, hoping that the answer will come eventually from careful interpretation of x-ray observations of supernova remnants. (Again see McKee and Hollenbach, 1980, for a discussion of progress to date.)

A second complication which has drawn considerable attention is the role of thermal conduction in supernova remnants (e.g., Solinger, Rappaport, and Buff, 1975; Chevalier 1975, 1977; Cowie, 1977). This is particularly important in that thermal conduction, if it were as

important as straightforward estimates indicate that it could be, would ruin the assumption of adiabaticity which underlies the entire treatment of §I.

Such an estimate of the importance of thermal conduction can be made by assuming the adiabatic structure, calculating the thermal conduction flux expected, and assessing its effect on the jump conditions of the shock. The modified jump conditions are given by $x_s^2\,[1 + (2F/\rho_0 v_s^3)] = 5\,x_s - 4$ where F is the arriving thermal conduction flux per unit area. Thus $x_s = 2$ follows from $F = \rho_0 v_s^3/4$, and $x_s = 3$ from $F = \rho_0 v_s^3/9$. Clearly a very modest conduction flux is sufficient to alter details of the structure considerably. For the early adiabatic blast wave, $p \propto R^8$, $n \propto R^{12}$ near the edge, so $T \propto R^{-4}$ and $-\partial T/\partial R = 4T_s/R_s$.

Taking $\kappa = 6 \times 10^{-7}\, T^{5/2}$ cgs, and defining $\delta = 9F/(\rho_0 v_s^3)$ as a measure of the significance of thermal conduction, assuming the Sedov evolution, we have

$$\delta = \frac{36\,\kappa\,T_s}{\rho_0 v_s^3 R_s} \simeq \frac{3.2\,\kappa}{n_0 k v_s R_s} \simeq 0.16\,\frac{E_{51}^{3/5}}{n_0^{8/5}\,t_4^{14/5}} \propto R_s^{-7} \tag{26}$$

where $t_4 = t/10^4$ yr. Three conclusions are evident: (1) If $\delta \gg 1$ in this formula, the thermal conduction is saturated so that the true ratio is of order unity; (2) if $\delta \ll 1$, thermal conduction has little effect on the expansion, although its effects in the remnant interior are somewhat more persistent; (3) the changeover from large to small δ, marking the fading of thermal conduction significance, occurs precipitously (measured particularly by R_s dependency) at a time

$$t_{mech} \simeq 5200\ \text{yr}\ E_{51}^{3/14}/n_0^{4/7} \simeq t_{eq} \tag{27}$$

when $\delta = 1$ and $x_s \simeq 3$.

There are several distinct situations which warrant discussion:

1. The magnetic field within a remnant may interfere with thermal conduction to a degree that the evolution is essentially adiabatic.
2. Electrons may be heated only by coulomb collisions, in which case they gain access to the energies of the ions (at t_{eq}) only as their ability to redistribute that energy is waning (at t_{mech}). Their influence on the structural evolution is then never very great, but prior to t_{eq} the ion gas is nearly adiabatic, the electron gas nearly isothermal, and $T_e < T_s$. After t_{eq}, the temperature structures merge just as adiabaticity becomes a reasonable approximation for the single fluid.
3. If electrons were heated to the ion temperature at the shock front, even for $t < t_{eq}$, saturated conduction would lead to a modest enhancement of the flux arriving at the front, decreasing x_s and increasing the shock speed somewhat. The greater significance of the conductivity in the center would lead to a significant flattening of the electron temperature distribution. Once again, however, the electrons in the interior would not have access to the ion energies for $t < t_{eq}$. Hence the flattening of T_e would not lead to a similar flattening of either the ion temperature or the density distribution (Cowie, 1977). Once again for $t < t_{eq}$ the ion fluid would be nearly adiabatic, the electron fluid nearly isothermal, but the two would have the same temperature at the shock. As $t \to t_{eq}$, the electrons would be heated by the ions, but the importance of thermal conduction thereafter would be small.

4. If electrons were not only heated at the shock but some process existed to keep the electron and ion temperatures equal thereafter, then for $t < t_{mech}$, both electron and ion temperatures would be flattened by conductivity and there would be a density plateau in the interior (c.f. Chevalier, 1975). Thus at early times, a description based on the assumption of adiabaticity would be inappropriate, although the radiative properties would not be drastically different (e.g., Solinger, Rappaport, and Buff, 1975; Gronenschild and Mewe, 1979). For $t > t_{mech}$, an adiabatic description would gradually become appropriate.

In the remainder of this paper, we will consider only two models, one with only coulomb heating of electrons, and one with $T_e = T_i = T$ everywhere. Both models are adiabatic. The former is appropriate for possibility 2 above, whether or not the magnetic field quenches thermal conductivity. It also approximates possibility 3 for $t > 0.6\ t_{eq}$ because, as shown by Itoh (1978) and §IIC below, this case leads to a flat electron distribution which rises to the shock temperature at $0.5\ t_{eq}$, providing a structure similar to that for possibility 3 for this and later times.

The second model is appropriate for either possibility 3 or 4 if thermal conduction is quenched by the magnetic field, but neither model describes either 3 for $t < 0.6\ t_{eq}$ or 4 for $t \leq t_{eq}$. The two models converge, as do all the possibilities, for $t > t_{eq}$.

B. Itoh's Formulation of Electron Heating

Itoh (1978) has shown that in an adiabatic flow with $T_e/m_e >> T_i/m_i$ and approximately constant value of $\ln \Lambda = \ln[1.2 \times 10^5 (T^{1/2}T_e/n^{1/2})]$, the evolution of normalized electron and ion temperatures, using Spitzer's (1962) formula for energy exchange by coulomb collisions, is independent of the history of a parcel of gas, once its conditions have been established at the shock front passage. Defining T as the average particle temperature (as found from adiabatic models which assume equal electron and ion temperatures), Itoh's result is that $g \equiv T_e/T$ is determined by

$$\left[\frac{3}{2} \ln \left(\frac{1 + \sqrt{g}}{1 - \sqrt{g}}\right) - \sqrt{g}(g + 3)\right]_{g_o}^{g} \approx \frac{\ln \Lambda}{81} \left(\frac{n}{T^{3/2}}\right) (t - t_o) \qquad (28)$$

where t_o is the time the particle was shocked, g_o is g just behind the shock, and $n/T^{3/2}$ is a constant established at the shock. The numerical form of this equation assumes cgs units, $n_{He}/n_H = 0.1$.

In order to find g(t), the above equation must be inverted. We have done this, approximately, by curve fitting with the result that the

equation

$$f = \frac{3}{2} \ln \left(\frac{1 + \sqrt{g}}{1 - \sqrt{g}}\right) - \sqrt{g}\,(g + 3) \qquad (29)$$

inverts to

$$g \simeq 1 - \exp\left[- \left(\frac{5}{3} f\right)^{0.4} \left\{ 1 + 0.3 \left(\frac{5}{3} f\right)^{0.6} \right\}\right] \qquad (30)$$

with an accuracy of better than 2% for $0 \leq g \leq 1$ (although 1-g is only this accurate for $g \lesssim 0.8$). The electron temperature is thus followed in time by evaluating f_o from equation (29), with $g = g_o$, adding the right hand side of (28) to f_o and substituting the result in (30). The validity of the procedure depends almost exclusively on adiabaticity.

C. Application of Itoh's Formulation to Kahn's Results

The previous results can be applied directly to obtain the electron temperature distribution in the central regions of a strong adiabatic blast wave. For this material, the initial ion temperature was extremely high so we take $g_o = 0$. In addition, this material was shocked at a time $t_o(R)$ very much less than the present age of the explosion (in order now to be found near the center).

Hence

$$f_{center} \approx \frac{\ln \Lambda}{81} \left(\frac{n}{T^{3/2}}\right) t. \qquad (31)$$

Also near the center, $n/T^{3/2}$ is very small so equation (30) can be approximated (for $f \lesssim 0.1$) by

$$g_{center} \approx (\frac{5}{3} f)^{2/5} \tag{32}$$

whereupon

$$\frac{T_e}{T}\Big|_{center} \approx [\frac{\ln \Lambda}{49} (\frac{n}{T^{3/2}}) t]^{2/5} . \tag{33}$$

From equations (14) and (16) with $x_s = 4$, the density distribution near the center is

$$\frac{n}{n_o}\Big|_{center} \approx \frac{5}{2} e^{-9/16} (\frac{R}{R_s})^{9/2} \tag{34}$$

from which the initial location, R_i, of a parcel now found at R can be evaluated to have been

$$\frac{R_i}{R_s} \approx e^{-3/16} (\frac{R}{R_s})^{5/2}. \tag{35}$$

The initial mean post-shock temperature of this material was

$$T_i = T_s(\frac{R_s}{R_i})^3 = T_s e^{9/16} (\frac{R_s}{R})^{15/2} \tag{36}$$

where T_s is the present post-shock mean temperature. This material has, however, been adiabatically decompressed from $4n_o$ to n so that its present temperature is

$$T = T_1\left(\frac{n}{4n_0}\right)^{2/3} \simeq T_s\left(\frac{5}{8}\right)^{2/3} \; e^{3/16} \left(\frac{R_s}{R}\right)^{9/2}. \tag{37}$$

Substituting equations (34) and (37) into (33),

$$T_e \simeq \left[\frac{\ln \Lambda}{49} n_0 T_s \frac{5^{5/3}}{8} e^{-3/8} t\right]^{2/5}, \tag{38}$$

which result is independent of R! The existence of this central plateau in T_e has in fact been found previously in the (corrected) numerical study of Itoh (1978) and in that of Gronenschild and Mewe (1979). Equation (38), however, predicts the value of this plateau temperature analytically through a combination of Itoh's and Kahn's approximation schemes.

Instructive manipulations of equation (38) can be made by eliminating either T_s or t using the blast wave evolution of equations (4). For $\ln \Lambda \simeq 35$, the second of these yields

$$T_e\,|_{\text{plateau}} \simeq 1.4 \times 10^7 \text{ K } (T_s/10^6 \text{ K})^{1/15} E_{51}^{2/15} n_0^{4/15} \tag{39}$$

showing an extremely weak dependence on T_s. Eliminating $T_s \propto t^{-6/5}$ shows $T_e \propto t^{-2/25}$.

Since T_s is dropping more steeply in time than T_e, there comes a time when the nearly uniform electron temperature equals T_s. Shortly thereafter, a significant fraction of the mass obtains $T_e \simeq T_1$ so that this moment marks the onset of equilibration. With suitable substitutions (as above) in equation (38),

$$T_e\Big|_{plateau} \approx T_s \left[\frac{t}{2600\ yr} \frac{n_o^{4/7}}{E_{51}^{3/14}}\right]^{28/25} \qquad (40)$$

(again with $\ln \Lambda = 35$). As noted previously, the plateau T_e reaches T_s at $t = 0.6\ t_{eq}$. Finally, we note from equation (39) that the electron temperature for $t < t_{eq}$ (and therefore the highest expected at any time) depends almost exclusively on the density of the ambient (assumed homogeneous) medium.

D. Cooling of an Adiabatic Blast Wave

The cooling rate in and cooling time of a blast wave is a somewhat strange thing to contemplate estimating when the electrons are out of equilibrium with the ion temperature, and the ionization level distribution is even further out of equilibrium with T_e. As this section will show, however, an equilibrium calculation is reasonable when estimating the cooling time marking the end of the adiabatic era. Thus we begin with such a calculation.

The emissivity of a gas is usually defined as $L(T_e)n_e n_H$ erg cm^{-3} s^{-1} and values of $L(T_e)$ for a gas whose ionization level is in collisional equilibrium with T_e are fairly well known (e.g. Raymond, Cox, and Smith, 1976, hereafter RCS). Kahn (1975, 1976) has pointed out for the special case with $L \propto T_e^{-1/2}$ and $T_e = T$, that a freely cooling parcel of gas has a cooling time which is independent of the history. More specifically, $p/\rho^{5/3}$ reaches zero at a time which is independent of the separate histories of p and ρ. For $n = 1.1\ n_H$ and $n_e = 1.1\ n$, this cooling time is

$$\Delta t_{cool} = \frac{2.1\ kT}{L(T)n} . \qquad (40.5)$$

Furthermore, for the temperature range from 4×10^5 K to 5×10^7 K, the equilibrium cooling function of RCS is fairly well approximated by $L(T) \sim 1.3 \times 10^{-22}\ (T/10^6\ K)^{-1/2}$ erg cm^3 s^{-1} so that equation (40.5) gives a reasonable estimate of the cooling time for this material.

Assuming the appropriateness of equilibrium cooling, equation (40.5) can then be used (Kahn; 1975, 1976) to calculate the time at which each parcel of gas swept over by a strong blast wave in the adiabatic phase will eventually cool. The earliest cooling of any parcel then marks the effective end to the adiabatic phase. For a parcel encountered at time t_s when the post shock temperature was T_s, the cooling is complete at a time

$$\begin{aligned} t_{cool} &= t_s + \frac{2.1}{4}\ \frac{kT_s}{L(T_s)n_o} \\ &= t_1\ (\frac{t_s}{t_1}) + \frac{2.1}{4}\ \frac{kT_{s1}}{L(T_{s1})n_o}\ (\frac{t_s}{t_1})^{-9/5} \end{aligned} \qquad (41)$$

where t_1 is a fiducial time which we choose to equal the shock time of the first parcel to finish cooling. Setting $d(t_{cool})/dt = 0$ and $t_s = t_1$ at this moment, we find the condition

$$\frac{9}{5}\ \frac{2.1}{4}\ \frac{kT_{s1}}{L\ (T_{s1})\ n_o t_1} = 1 \qquad (42)$$

and $t_{cool} = (14/9)t_1$. Using the approximate RCS cooling function,

$$t_1 = \frac{9}{14} t_{cool} \approx 3 \times 10^4 \text{ yr } \frac{E_{51}^{3/14}}{n_o^{4/7}} \tag{43}$$

and

$$T_s(t_1) \approx 0.96 \times 10^6 \text{ K } (E_{51} n_o^2)^{1/7}. \tag{44}$$

Equation (44) verifies that the cooling is occurring at temperatures for which the approximation to L(T) is reasonably valid as long as $2 \times 10^{-3} < E_{51} n_o^2 < 8 \times 10^{11}$. Finally, comparing equations (43) and (25), $T_e \approx T$ is a very acceptable assumption well before cooling becomes appropriate, so that our attention can be concentrated on the effects of the non-equilibrium ionization structure.

We now proceed to an estimate of the non-equilibrium cooling coefficient behind a shock front. We note first that the radiation from ions of a given element will have a softer spectrum than in the equilibrium case because lower stages of ionization are present. Secondly, the net emissivity will be higher than in equilibrium, because these lower stages are more easily excited by electron collisions.

As an element enters the shock front, it is rapidly ionized through the lower stages and soon finds itself caught in a stage for which the ionization time is very long. This occurs because the ionization coefficients decrease very rapidly with increasing ionization stage. Thus the most prevalent stage of ionization will be that for which the ionization coefficient α_I is of order $1/(n_o t)$. These coefficients can be written (e.g. Cox & Tucker, 1969)

$$\alpha_I \simeq 1.3 \times 10^{-8} T_e^{1/2} \xi F \frac{e^{-I/kT_e}}{(I_{ev})^2} \text{ cm}^3 \text{ s}^{-1} \tag{45}$$

where ξ and F are factors of order unity. From this we can solve for the exponential factor

$$e^{-I/kT_e} \sim \frac{(I_{ev})^2}{1.3 \times 10^{-8} T_e^{1/2} \xi F n_o t} \quad . \tag{46}$$

The emissivity due to that element comes primarily from the collisional excitation of this ion at a rate (e.g. Cox and Tucker, 1969)

$$E\,\alpha_E \simeq 2.7 \times 10^{-15} T_e^{-1/2} f g e^{-E/kT_e} \quad \text{erg cm}^3 \text{ s}^{-1} \tag{47}$$

where again f and g are of order unity. Thus the cooling coefficient for this element can be written

$$L_i(T_e) \sim A_i (2.7 \times 10^{-15} T_e^{-1/2}) fg \left[\frac{(Iev)^2}{1.3 \times 10^{-8} T_e^{1/2} \xi F n_o t}\right]^{E/I} \tag{48}$$

where A_i is the abundance of the element relative to hydrogen. The ratio of strongest excitation line energy, E, to ionization energy, I, shows considerable variation among ions but generally lies in the range 0.25 to 0.75 and we take $E/I \sim 0.5$ as representative. We similarly take 0.1 to be characteristic of the quantity $fg/(\xi F)^{1/2}$, making

$$L_i(T_e) \sim 2.4 \times 10^{-12} A_i \frac{I_{ev}}{T_e^{3/4}} \left(\frac{1}{n_o t}\right)^{1/2} \text{erg cm}^3 \text{ s}^{-1}. \tag{49}$$

Finally, realizing that the reason the element became stuck in this stage of ionization is that I exceeded kT_e, we take $I \sim 1.5\ kT_e$ (which we can safely do when it is not in an exponential). Our final estimate is then

(summing over all heavy elements and taking $\Sigma A_i \sim 2 \times 10^{-3}$)

$$L(T_e) \sim 0.6 \times 10^{-18} T_e^{1/4} \left(\frac{1}{n_o t}\right)^{1/2} \text{erg cm}^3 \text{ s}^{-1}. \tag{50}$$

We now eliminate t using equation (4) and, assuming $T_e = T_s$, obtain the approximate non-equilibrium cooling coefficient for material just inside a strong adiabatic blast wave with hot electrons:

$$L(T_s) \sim 2 \times 10^{-27} T_s^{2/3} \left(\frac{1}{E_{51} n_o^2}\right)^{1/6} \text{erg cm}^3 \text{ s}^{-1}. \tag{51}$$

We note that the important scaling of collisional processes with $E_o n_o^2$ (c.f. Chevalier, 1974) has survived this estimation procedure. This scaling also appeared in equation (44).

The ratio of equation (51) to the approximated equilibrium coefficient is proportional to $T_s^{7/6}$ and equation (51) is projected to drop to the equilibrium value when $T_s = T_E$, $t = t_E$ with

$$T_E \sim 5 \times 10^6 \text{ K } (E_{51} n_o^2)^{1/7}$$

$$t_E \sim 7600 \text{ yr } \frac{E_{51}^{3/4}}{n_o^{4/7}}. \tag{52}$$

Checking back on the validity of the approximations leading to this result, we find that at time t_E, the quantity in square brackets in equation (48) is of order 0.1 so that the error introduced by the uncertainty in E/I is no greater than the general factor of 3 or so uncertainty from the choice of parameters. The combination of parameters

introduced above normalizes equation (50) to agree very well with the detailed machine results of §III.

Since the true non-equilibrium cooling rate is always higher than that for equilibrium, we can interpret the above results to imply that for $t > t_E$, the equilibrium rate should be reasonably appropriate. And since $t_E \sim 1/4\ t_1$, we would conclude from this argument that equation (43) can be used to reliably predict the end of the adiabatic phase of a $p_o = 0$ blast wave.

To test this conclusion, we now approach the question of ionization equilibration more directly. If, at temperature T_s, a particular element in collisional equilibrium has z as its dominant ionization stage, and that stage has ionization coefficient $\alpha_I(z)$, then this element should be close to ionization equilibrium only if $4.4\ n_o\alpha_I(z)t$ is large compared to 1. The dominant stage at any temperature is the one with most nearly equal ionization and recombination coefficients. If radiative recombination dominates, it is straightforward to show that this would imply that $I(z)/kT$ would be about 10 (varying slowly from about 13 at $z = 1$, to 9 at $z = 10$), and that both the ionization and recombination coefficients would be roughly $2 \times 10^{-11}\ z^2 T^{-1/2}\ cm^3\ s^{-1}$. For most stages of ionization, $I(z) \lesssim (z+1)^2\ I_H$, where $I_H = 13.6$ eV, making $(z+1)^2 \gtrsim I(z)/I_H \sim 10kT/I_H \sim 6.3 \times 10^{-5}\ T$. Ignoring the difference between z and z+1, the characteristic ionization and recombination rates would be $\alpha_{CE}(T) \sim 1.2 \times 10^{-15} T^{1/2} cm^3 s^{-1}$. This, however, is a lower limit, owing to our neglect of dielectronic recombination which pushes the equilibrium ionization level downward at a given temperature. This sometimes considerably enhances the characteristic ionization rates, and shortens

the time required to establish equilibrium. We thus take the above value as the minimum rate at which equilibrium is established.

The minimum degrees of equilibration at times t_E and t_1 are thus measured by $4.4\ n_o \alpha_{CE}\ (T_E) t_E \sim 3(E_{51} n_o^{\ 2})^{3/14}$ and $4.4 n_o \alpha_{CE}\ (T_s(t_1)) t_1 \sim 5(E_{51} n_o^{\ 2})^{3/14}$ respectively. The implication is that at least for $(E_{51} n_o^{\ 2}) \gtrsim 1$, collisional equilibrium is nearly valid by the time significant cooling begins, supporting the collection of cooling time estimates which have been made for normal supernova remnants on the basis of equations like (43).

For ambient densities substantially lower than 1 cm^{-3}, we have not so far succeeded in assessing the degree of collisional equilibration which occurs before time t_1. We note, however, from equation (44) that the post shock temperature at time t_1 decreases slowly with decreasing $(E_{51} n_o^{\ 2})$, and is less than 10^6 K at the densities whose equilibration is in question. It is further true that the difficulty with equilibration is generally most severe when ionization of the K-shell of abundant elements is involved, because of the large jump of ionization potential at the helium-like stage. The production of the helium-like stage, however, occurs readily owing to the ease with which the lithium-like stage is stripped of its last L-shell electron. Finally, for temperatures below about 1.5×10^6 K, 10^6 K, and 6×10^5 K, the abundant elements oxygen, nitrogen, and carbon, respectively, are no longer ionized beyond the helium-like stage in collisional equilibrium. Hence, for $T_s < 10^6$ K there is a rapid increase in the ease with which equilibrium is approached. This should remain true down to $E_{51} n_o^{\ 2} \sim 1.3 \times 10^{-5}$, $n_o \sim 5 \times 10^{-3}\ cm^{-3}$ at which point the complete ionization of

helium can no longer be assured; but at such low densities, the effects of the ambient pressure and pre-ionization level can no longer be neglected. Thus for all cases in which we would be interested in applying the cooling time formula, collisional equilibrium should be fairly well approached before significant cooling sets in. Of course there will always be a region just inside the shock front in which the ions are scrambling towards equilibrium and where the emissivity is high, but the added cooling rate from this layer dwindles with time.

Finally, by comparing equations (25), (27), (43), and (52) we find that, for a strong (p_o = 0) blast wave, t_{cool}, t_1, t_E, t_{mech} and t_{eq} are always found in the ratios 9.3: 6: 1.5: 1.0: 1.0 as an incontrovertible sequence and conclude that equation (43) solved for t_{cool} reliably denotes the end of the adiabatic evolution and the onset of shell formation.

III. Ionization Structure and Luminosity

A. Procedure for Finding the Ionization Structure

The previous sections provide good analytical approximations for the dynamical structure of an evolving adiabatic blast wave for $R_s \leq 1.7\ R_c$. In order to find the spectrum of such an explosion, however, the ionization structure must be known at each location and this can only be found by following the individual gas parcels' histories from the time they are shocked until the moment when the spectrum is to be evaluated. For each such history, the time derivatives of each stage of ionization of each atomic species must be integrated numerically. Such computations have recently been carried out for strong blast waves (negligible external pressure) by Itoh (1979) and by Gronenschild and Mewe (1979). The procedure used here for the integrations follows that outlined in Cox (1972) and will not be discussed in detail. The ionization and recombination rates used are those of Raymond and Smith (1977).

We found it useful to choose the parcels to follow, not by the radius at which they were located, but by the post shock pressure, y_{si}, when they were first struck by the shock. The suitable distribution of these pressures was chosen to be sharply peaked near the final post shock pressure, y_{sf}, at the moment the spectrum is to be evaluated. This was necessary in order to resolve the rapidly changing conditions near the edge. Thirty parcels in all were followed.

Once y_{si} is chosen, the initial compression, x_{si} follows from equation (19) and the initial location of the mass, R_i (the shock position when $y_s = y_{si}$), is given by equation (11). The time, t_{si}, is

found from equation (23). The evolution of each parcel in time was followed by subdividing the pressure drop $y_{si} - y_{sf}$ into 24 intervals (with smaller intervals at first and larger ones as $y_s \to y_{sf}$) and following conditions in the parcel as the shock moved outward and the post shock pressure dropped through the sequence of intervals.

At an epoch when the post shock pressure is given by y_s, conditions in the parcel of interest can be found only after the parcel is located. This location follows from knowing R_s from equation (11) and since $\mu = (R_i/R_s)^3 = r_i^3$ for the parcel, equation (15) becomes

$$r_i = r^{5/2} \exp\left[\frac{(x_s - 5/2)}{q}(r^q - 1)\right]. \tag{53}$$

In this equation, x_s and q follow from equations (2) and (14) with the current value of y_s. The inversion of equation (53) to find $r(r_i)$ is facilitated by rewriting it as

$$\begin{aligned}&\left(\frac{2}{5}x_s - 1\right) \exp\left(\frac{2}{5}x_s - 1\right) r_i^{2q/5} \\ &= \left[\left(\frac{2}{5}\right)x_s - 1\right) r^q] \exp\left[\left(\frac{2}{5}x_s - 1\right) r^q\right]\end{aligned} \tag{54}$$

which is of the form $B = Ae^A$ where B is known and A desired. For $4 \geq x_s \geq 2$ and $1 \geq r_i \geq 0$, the range of B is $1.1 > B > -0.2$. The inversion proceeds easily by iteration with $A_0 = B/(1 + 0.763\ B)$, $A_{i+1} = B \exp[-A_i]$.

In calculating the spectrum, this procedure is also used to locate the boundaries of the gas parcels and differences taken to find their

volumes. For parcels very close to the shock front, these volumes are very small (by choice) so that the number of iterations required to find r to sufficient accuracy can be fairly large.

Once A, and therefore r are found for the parcel, the density is found from equation (16), the pressure and mean temperature from equation (20), and the time from equation (23). In models for which the electron and ion temperatures were assumed equal, nothing more was required to follow R(t), n(t), and $T_e(t)$ for the parcel, and the ionization equations can be integrated. We assumed that the ions outside the shock were in collisional equilibrium with T_o, the external ambient temperature, as the initial conditions for the integration.

For those models in which electrons were assumed to be heated only by coulomb collisions, the post-shock electron temperature was taken to be T_o, so that $g_o = T_o/T_{si}$. (In the future, we plan to use a post shock electron temperature equal to $T_o(x_s)^{2/3}$ to allow for the adiabatic compression.) Then f_o is evaluated from equation (29). At all subsequent times,

$$f = f_o + \frac{\ln \Lambda}{81} \left(\frac{n}{T^{3/2}}\right) (t - t_{si})$$

$$= f_o + 0.43 \frac{n_o}{T_o^{3/2}} \left(\frac{x_{si}^5}{y_{si}^3}\right)^{1/2} (t - t_{si}) \qquad (55)$$

with $\ln \Lambda = 35$ appropriate for the cases we explore here. Thus $g = T_e/T$ is found from equation (30); T is found from equation (20) as before, and the determination of $T_e(t)$ is completed. The integration of the ionization equations can then be carried out.

B. Program Capabilities

The procedures outlined above were written into a computer program designed to start with the ambient medium in collisional equilibrium with temperature T_o, density n_o, and given elemental abundances, and to perform the necessary calculations to describe a blast wave of energy E_o at one epoch, characterized by y_{sf}. At that epoch, the program provides R_s, t, y(r), x(r), T(r), T_e(r), all ionic concentrations as functions of r, the column densities of all ions from near the explosion center to the edge, the total spectrum (distributed in 5 eV bins), and the total luminosity (emissivities use the calculated ion concentrations with the emission rate coefficients of Raymond and Smith, 1977). It furthermore calculates the spectral distribution of surface brightness of 3 rays through the object, one passing through r = 0, and ones tangent to r = 0.5 and 0.9. Finally, for comparison, it recalculates the ionic concentrations, column densities, spectrum, luminosity, and surface brightness spectra which would result if the ions were in collisional equilibrium with T_e. The program can be switched to run either with coulomb heating of electrons, or with $T_e = T_i = T$, but is adiabatic in either case. As mentioned previously, the results should be appropriate for $x_s \geq 2$, $y_s \geq 3.5$ so long as radiative cooling causes only negligible perturbations of the structure. For strong shock waves the latter condition requires $t < t_1$ as given by equation (45). This condition is modified by significant ambient pressure but can be roughly summarized by the requirement that $\mathcal{E}t$ must be small compared to E_o.

Eleven diagnostic runs were made with this program and some of the results are discussed in the remainder of this paper.

C. Runs Performed and Their Luminosity Evolution

We are particularly interested in applying this program to a study of the soft x-ray background, and this has biased our initial set of calculations toward very low ambient densities and large scales. The actual runs which have been performed thus far are shown as 3 groups in Table 1. In group A, we followed the time evolution of an explosion of 5 x 10^{50} ergs into $n_0 = 5 \times 10^{-3}$ cm^{-3}, $T_0 = 5 \times 10^5$ K assuming that only coulomb collisions heat the electrons. This explosion was studied at four times bracketing t_{eq}. In addition, it was restudied at two of the times with the alternative model, $T_e = T_i = T$.

In group B, we studied three situations which differed initially only in their ambient temperatures. All had the same energy and ambient density and were examined at the same shock radius. All had $t \sim t_{eq}$ as defined for $p_0 = 0$ evolutions by equation (25). The differences in T_0, however, resulted in differences in T_s, t, and all of the other parameters to some extent, which, as we shall see, caused variations of equilibration across this group. All three runs were made assuming that only coulomb collisions heated the electrons, but one was repeated with $T_e = T_i = T$. Within this group, run 31E was not entirely well-behaved, showing some jumpiness in its properties. We include the results here because they contain information not present in other runs, but the detailed results should be considered as tentative.

Group C consisted of only one run, with parameters similar to idealized symmetric models of the Cygnus Loop (exclusive of the dense filaments). For both this example and run 4E of group A the equilibrium cooling rate was expected to be appropriate. As we shall see, this

prediction is not supported in detail by the model results.

Also shown in table 1, are the post shock temperature, the electron temperature for the innermost zone, the calculated total luminosity, the total luminosity which would have been found if the ion concentrations had been in collisional equilibrium with T_e, and hand calculated estimates of the latter two quantities.

The estimated luminosities were derived in the following way. The true luminosity is

$$\mathcal{L} = \int_0^{R_s} 4\pi R^2 [n^2 L] \, dR \tag{56}$$

where L is the local cooling coefficient which depends on T_e and all of the ionic concentrations. We assumed that this could be approximated by

$$\begin{aligned} \mathcal{L} &\approx L(T_e') \int_0^{R_s} 4\pi R^2 n^2 dR \\ &\approx 2.06 \left[\frac{4}{3} \pi R_s^3 n_o^2 \right] L(T_e') \end{aligned} \tag{57}$$

where the compaction parameter of 2.06 was found from a numerical integration over Kahn's approximation to the Sedov solution. Here $L(T_e')$ is the cooling coefficient at a representative electron temperature. We chose T_e' as the post shock temperature or the innermost zone electron temperature, whichever was lower.

To estimate the non-equilibrium luminosities, we took $L(T_e')$ from equation (50) with the result that for $t < t_E$,

$$\mathcal{L} \sim 4.8 \times 10^{39} \left(\frac{R_s}{100\ \mathrm{pc}}\right)^3 \left(\frac{n_o}{1\ \mathrm{cm}^{-3}}\right)^{3/2} \left(\frac{T_e'}{10^6\ \mathrm{K}}\right)^{1/4} \left(\frac{10^{12}\ \mathrm{s}}{t}\right)^{1/2} \mathrm{erg\ s}^{-1}, \quad (58)$$

whereas the approximation to the RCS cooling function presented in §IID was used for the collisional equilibrium luminosities to give

$$\mathcal{L}_{CE} \sim 3.3 \times 10^{40} \left(\frac{R_s}{100\ \mathrm{pc}}\right)^3 \left(\frac{n_o}{1\ \mathrm{cm}^{-3}}\right)^2 \left(\frac{10^6\ \mathrm{K}}{T_e'}\right)^{1/2} \mathrm{erg\ s}^{-1}. \quad (59)$$

In comparing these estimates with the machine results, three points should be borne in mind. At early times ($t < t_{eq}$), T_e' overestimates the representative electron temperature for the coulomb heating cases. In addition the assumption of a constant compaction parameter breaks down when T_s/T_o is not large, causing overestimated luminosities at late times. Thirdly, the very uncertain normalization of equation (50) was adjusted once the machine results were in hand to make equation (58) as accurate as possible.

The estimates, by and large, are very good. No CE estimate errs by move than 40%; these estimates improve as $t \to t_{eq}$ as expected from above. For the $T_e = T_i$ cases, the CE errors are less than 10%. For seven out of the 11 runs performed, the estimated nonequilibrium luminosities are also within 10% of the machine results, although it is clear from the run series 3E, 2E, 1E, 4E, that there is a gradual increase in the ratio of true to estimated luminosity. This drift could be removed if the typical value of E/I were taken as 0.37 rather than 0.5 in deriving equation (50). This would then lead to $\mathcal{L} \propto R_s^{3} n_o^{1.63} (T_e')^{0.055} t^{-0.37}$. When normalized to run 2E, this revision removes the drift in

group A, but alters the estimates for groups B and C by less than 5 and 20 percent respectively, far less than would be required to overcome the significant discrepancies in 3 of the 5 runs.

In addition, such an adjustment in the estimate leads to a false comfort that the luminosity evolution is fully understood in terms of the previous discussion. For run 4E, the compaction parameter is less than 2.06 (as evidenced by low T_s/T_o and the estimated $\mathcal{L}_{CE}$ exceeding the machine result), and the luminosity estimate should be too high. For this run, however, the true luminosity is anomalously high just as it should be approaching the equilibrium rate. We believe that the reason for this depends on a detail: at the T_s of run 4E, carbon would be fully ionized in equilibrium, but, in the flow, retains one or two K-shell electrons. The additional cooling due to these ions keeps the non-equilibrium rate higher than the equilibrium value until T_s drops enough that carbon also has K-shell electrons in equilibrium. This same effect is seen exaggerated in run 21E where T_s is high enough that oxygen performs this same function. Further discussion of this effect is found in Gronenschild and Mewe (1979).

Finally the differences between the machine results and estimates of $\mathcal{L}$ for runs 31E and 41E can be understood in terms of the effects of T_o on the ionization just inside the shock and is discussed briefly in the footnotes to the table. For cases 31E and 21E, both with low T_o, the magnitude of discrepancy may partly be due to poor resolution of the low stages of ionization near the edge, or to incomplete stripping of helium.

We have emphasized the discrepancies in this discussion, because they draw our attention to additional considerations in the physics. This would not be possible, however, if the overall quality of the estimates were not so high. The worst disagreement appears to be for run 31E but, as we shall see, the agreement even for this run is quite good if we limit our attention to x-ray energies.

D. Some Details of Two Runs

Both Itoh (1979) and Gronenschild and Mewe (1979) have discussed the dynamic, thermal, ionization, and spectral structure of blast waves into negligible ambient pressure. We now present the details of two of our runs, reviewing the principal conclusions of the earlier papers in the process.

The runs chosen for this comparison are numbers 11E and 11 from group B, differing only in their assumptions about electron heating. (As will be seen in §IV, these two runs have parameters compatable with the soft X-ray background model.) The dynamical structures of these two are identical and are shown in Figure 2a,b. The post shock compression factor is $x_s = 3.05$, the pressure enhancement $y_{sf} = 11.76$. The effects of the ambient pressure on the structure are beginning to be felt at this epoch ($R_s = 102$ pc, $R_c = 106$ pc). The mean temperature distribution is also the same for both runs, shown as a solid line in Figure 2c. In run 11, this is also the electron temperature; but for run 11E, the electron temperature is shown as a dashed line. Clearly this case is on the verge of equilibration of T_e, the interior electron temperature just slightly exceeding T_s. From equation (40) this thermal structure is predicted to occur for

the $p_o = 0$ solution when $t \sim 0.6\ t_{eq}$ whereas this run actually has $t \sim t_{eq}$ as given by equation (25). Thus equilibration has been delayed by the lower compression and higher T_s brought about by the higher external pressure. Notice in Table 1 that run 31E, identical except for its low T_o, has in fact equilibrated at this stage of development.

The distributions of ionization stages for oxygen are shown in Figure 3a,b. The initial concentrations, equilibrium at 5×10^5K, were approximately 90% O^{+6}, 7.5% O^{+5}, and 2.5% O^{+4}. The rapid disappearance of O^{+4} behind the shock is evident in both cases; O^{+5} follows a similar but slower decline. Had T_o been lower; much of the oxygen in the dense edge region would have been O^{+5}, with O^{+6} being the ionization stage in which the element then became stuck (in the sense of §IID). For run 11E, this sticking continues far into the interior, whereas for run 11, there is gradual conversion to the hydrogen-like ion, and even some complete stripping. This difference follows from the fact that the interior electron temperatures are much higher in the latter case, and were significantly higher yet in the past when this inner material was in the dense region near the edge. For run 11E, T_e is nearly uniform in position and constant in time so that the ionization level depends primarily on $\int n_e dt$ of each gas element. This integral is small near the edge, for newly shocked material, and small in the center for material which was shocked early but spent little time at high densities. Both runs, in fact, show a peaking of the ionization level some distance interior to the shock, but for run 11, this occurs farther inward than for 11E because of the higher electron temperature history of the former.

The distribution of the equilibrium ionization structure of oxygen

is not shown, but it consists of a larger proportion of the hydrogen-like and bare ions. For fairly light elements at these temperatures, the equilibrium is largely bare nuclei whereas the non-equilibrium case gets stuck trying to ionize the K-shell. For elements which are significantly heavier than oxygen, the K-shell is not reached in either case and the equilibrium and non-equilibrium distribution peaks can differ by several stages of ionization. For more complete discussions see Itoh (1979) and Gronenschild and Mewe (1979).

Four of the surface brightness spectra produced by these two runs are shown in Figure 4. These specific spectra are from a line integral through the center

$$S(E_i) = 2 \int_0^{R_s} \frac{\epsilon(E_i)}{4\pi} \, dR \qquad (60)$$

where $\epsilon(E_i)$ is the local emissivity of the energy bin characterized by E_i. These emissivities include line and continuum contributions summed in 500 bins of 5eV width. Thus a bin which stands a factor of 100 above the neighboring continuum has an equivalent width of 500eV. The four figures are the non-equilibrium (i.e. actual) and collisional equilibrium spectra of both runs. Note the differences in vertical scales.

The major features of these diagrams can be summarized as follows:

1) Lines dominate the luminosity for all four.

2) The $T_e = T_i = T$ case (#11) has significantly more emission at high energies from the significantly higher electron temperature, and an upward curvature of the continuum from the hotter interior.

3) The equilibrium continua show more pronounced recombination

edges from the high stages of ionization whereas the non-equilibrium continua show more pronounced two photon contributions from collisional excitation of, for example, O^{+6} to a metastable level.

4) The equilibrium spectra show significantly stronger lines from higher stages of ionization (appearing at high energies) than do the non-equilibrium spectra.

As before, the reader is referred to Itoh (1979) and Gronenschild and Mewe (1979) for more complete discussions.

IV. Application to Model the Soft X-ray Background

A. The Implied Parameters of the Local Emission Region

The suggestion has been made, (e.g. McKee and Ostriker, 1977), that much of the soft X-ray background might arise from our being inside a very large supernova blast wave propagating in the hot, low density component of the ISM. This is a refinement of the notion of Cox and Smith (1974) that the background arises in typical material of the hot component, and this refinement lowers the inferred temperature and pressure requirements of typical locations at the expense of putting the solar system in an atypical region. Such atypical regions certainly exist, however, and the likelihood of being within one is not negligible. We have thus undertaken this project to explore that suggestion quantitatively. We stress, however, at the outset that the models we present do not correspond to those envisioned by McKee and Ostriker (1977) because the medium modeled does not have the large number of small clouds undergoing thermal evaporation as in their view. Although we dispute their point of view elsewhere for the ISM as a whole (Cox, 1979), for the present purposes we simply note that there is no evidence for there being such clouds, or even a typical amount of neutral hydrogen, within 100 pc from the sun. We thus model the explosion as an adiabatic blast wave.

The gross features required for the disturbance come either directly from the observations, or from comparisons with the equilibrium emissivities of Raymond and Smith (1977) for a hot plasma. Detailed discussions are found, for example, in Burstein, Borken, Kraushaar, and

Sanders (1976); Sanders, Kraushaar, Nousek, and Fried (1977); Nousek, Fried, Sanders, and Kraushaar (1981); Fried, Nousek, Sanders, and Kraushaar (1981); Cox (1977); Kraushaar (1979); and McCammon, Kraushaar, Sanders, and Burrows (1980). The basic results are that the temperature of the emitting gas (from the observed spectrum) must be $\sim 10^6$ K; the radial scale of the emitting region must extend to at least 100 pc (from the observed anticorrelation with moderate column densities of HI); and the likely emission measure $\int n_e^2 dr$ is $\sim$ 1 to 2 x 10^{-3} cm^{-6} pc. Thus to first order, the density is about 4 x 10^{-3} cm^{-3}, $p/k \sim 8000$ cm^{-3} K. Finally, the thermal energy contained in the nearest 100 pc is roughly 3 x 10^{50} ergs, which is approximately the energy of one supernova explosion. It is this last result, of course, which makes this project tempting.

A little manipulation leads to an estimate of the likelihood of being found within such a region. If the post shock temperature is roughly 10^6 K, the shock speed is about 300 km s^{-1}. The age of an adiabatic blastwave is $t = (2/5)(R_s/v_s)$ or 1.4 x 10^5 years for R_s = 100 pc, $T_s = 10^6$ K. If SN occur in the low density phase with a rate of 1 per 100 years, there should be about 1400 in the Galaxy as young as the one envisioned here, most of them nearly as old and large as this one. Thus such remnants occupy a total of about 10^{65} cm^3 of the galactic disk, or about 1 part in 40 of a disk with radius 15 kpc and thickness 200 pc. Their typical center to center separation, if positioned randomly in such a disk, would be about 500 pc. Thus the chances of a random point being located within such a disturbance are only of order 1 in 40 although the chance of being within 200 to 300 pc of the center of one or more is essentially unity. Finally, we note that the supernova reheating of a

preexisting cavity of this size bounded by a dense shell can resemble the model under discussion but have a significantly longer lifetime. Such models have been proposed for Loop I (Borken and Iwan, 1977) and for a region extending from Barnard's Loop to Eridanus (Reynolds and Ogden, 1979) and may eventually be found to describe best our local region as well.

B. Comparison of X-ray Observations with Model Results

The diffuse background data of the Wisconsion soft X-ray astronomy group is presented as count rates in a set of bands defined by a combination of window transparencies, counter response functions, and pulse height limits. Although detailed pulse height spectra are also obtained, the spectral resolution is such that most of the information is carried in the band count rates. Three of these bands, arranged in order of increasing mean energy have been named B (for boron filter), C (for carbon filter), and M (for medium energy). For these bands, count rate maps of the entire sky are approaching completion. Tentative maps for 80% of the sky can be found, for example, in McCammon et. al. (1980). More precise definitions of the bands are in Burstein, et. al. (1976).

The B, C, and M bands are sensitive, respectively, to photons in approximately the ranges 100 to 188 eV, 150 to 284 eV, and 450 to 1000eV. The count rates in these bands vary over the sky, but typically have values of order 50, 200, and 100 counts per second, respectively, in directions away from bright sources. The minimum values for these rates are about 30, 80, and 50 counts per second.

The soft X-ray astronomy group has programs which model the response of their instrument to input spectra, calculating the band count rates which would be seen for an incident surface brightness spectrum. Burstein, et. al. (1976), for example, have presented the results of such calculations using collisional equilibrium input spectra from Raymond and Smith (1977). The results are conveniently presented in band fraction diagrams (analogous to color-color plots or chromaticity diagrams) and as the required emission measure to achieve a given count rate.

The spectral results, summarized briefly, are that for temperatures below about 10^6 K very little M band is produced but B and C bands are copious, the ratio of B to C increasing with decreasing T. For temperatures above about 10^6 K, M band and C band are bright, M/C increasing with increasing temperature, but little B band is produced. A temperature can be found at which B/M is as observed, but the predicted C band is then much too bright. Thus the equilibrium models are driven to the assumption that two temperatures are required, one higher than 10^6 K to produce most of the M but only part of the C, and one lower than 10^6 K to produce most of the B band and the remaining portion of the C rate.

Nousek et al. (1981) have suggested that the hot component could be distantly located, such as in the galactic corona. From spectral studies of the lower energy bands in directions of varying hydrogen column density, however, it appears that most of the emission sensed by the B and C bands arises closer than the nearest 1×10^{20} atoms cm^{-2} of hydrogen, generally within 100 to 200 pc. The possibility that the M band emission alone arises from more distant regions is consistent with the rather close correlation between variations in the B and C band sky maps, and the lack of correlation of

these two with the more uniform M band map. Thus, for the present program, our goal is to account for the B and C band rates, with the observed M band rate as an upper limit.

The central chord surface brightness spectra calculated for the runs in Table 1 were divided by two and folded through the counter response of the soft X-ray counter to simulate the appearance of such blast waves viewed from within. The fact that we are unlikely to be found dead center is of little consequence since most of the emission arises near the edge, and surface brightness is distance independent. The resulting band count rates are shown in Table 2 along with the integrated O^{+5} column densities. Note that the count rates are shown for both the actual time dependent ionization structures and for the hypothetical equilibrium ionization distribution, for comparison.

The total surface brightness of these models should be proportional to $\mathcal{L}/R^2$. In fact, for all of the models with $T_0 = 5 \times 10^5$ K, the carbon band count rates of Table 2 are given within 6 percent by

$$C = 15.6 \left[\frac{\mathcal{L}}{10^{35} \text{ erg s}^{-1}}\right] \left(\frac{100 \text{ pc}}{R_s}\right)^2 \text{ counts s}^{-1} \qquad (61)$$

This accuracy must depend on the carbon-band-sensitive photons accounting for a large proportion of the total luminosity, or at least a nearly constant proportion.

The exceptions to the above behavior are easily understood. For runs with low T_0 (31E, 21E), the total luminosity is enhanced by the presence of low stages of ionization which do not radiate in the carbon band. For run 31E, however, equation (61) applies if the predicted luminosity from

equation (58) is used rather than the very high machine result. For run 21E, the carbon band is intermediate in brightness between the values obtained from the predicted and machine calculated luminosities. Apparently the carbon band is enhanced somewhat by the low T_0, but not by as large a factor as $\mathcal{L}$ as a whole. For the one run (41E) with a higher T_0, the converse behavior is found. The carbon band is less suppressed by the higher T_0 than is $\mathcal{L}$. Nevertheless, for runs 41E and 21E, equation (61) using predicted luminosities from equation (58) gives carbon band count rates within 14 and 37 percent respectively of the calculated values. Hence the carbon band rates in Table 2 are a reliable measure of the total surface brightness of the models with which to compare the B and M band rates.

The degree of ionization equilibration has a strong effect on the count rates. This can be seen by comparing the CE rates with the actual count rates. In all cases, the non-equilibrium rates exceed the CE values, the difference being significantly greater for B band than for C or M. By following the run sequences (3E, 2E, 1E, 4E) and (2,1), it is clear that this non-equilibration enhancement decreases with time, as expected. Within the set (31E, 11E, 41E), the enhancements are greater for larger T_0, but this can largely be accounted for just by the gradation in equilibration found earlier, with little additional effect depending on T_0 alone.

Since the C band rate evolves approximately as expected from the luminosity behavior, the ratios of band count rates M/C and B/C are sensitive to primarily two quantities: the temperature and the differential effect of equilibration. When the C and M band rates suffer

similar nonequilibration enhancements, as in the sequence (3E, 2E, 1E, 4E) the ratio of M/C should decrease in time due to the falling electron temperature. The B/C ratio, however, has competing tendencies. It increases as T_e declines, but decreases with increasing equilibration.

These effects are all seen in Table 3 which shows T_e', B/C, and M/C for all runs performed. For the run sequence (3E, 2E, 1E, 4E), M/C declines monotonically by a factor of about 3 as T_e' falls, while B/C shows a slight net increase, with fluctuations. For the runs (2,1) with $T_e = T_i$, M/C drops by a factor of 3 while B/C increases by only a factor of 1.4.

The B/C ratio thus shows little variation for the most part. For 8 out of the 11 runs, it lies between 0.34 and 0.46. It is somewhat lower for the only 2 runs (2,21E) which have $T_e' \geq 2.4 \times 10^6$ K and $T_e \approx T_i$. The only run with high B/C is 31E which has the lowest T_e', low T_o, and a somewhat questionable resolution of the edge in the model.

The M/C ratio, on the other hand, shows considerable variation in the models; but this variation is of little interest simply because the ratio is always much lower than that observed in the actual data. For only 2 runs does M/C exceed even 0.10. Run 2 with M/C = 0.13 has both a high T_e' and $T_e = T_i$. Run 21E, although not designed to represent the background, never-the-less reemphasizes the required parameters for achieving high M/C. This run, like run 2, has high T_e' and effectively $T_e = T_i$. Furthermore, it is closer to ionization equilibrium than run 2 which has a very high nonequilibrium enhancement of the C band. Thus 21E has a higher M/C than run 2 even though its T_e' is somewhat lower.

We are now prepared to compare the models with the data in a gross

sense. The first 6 runs of Table 2 all have C band count rates of about 160 per second, typical of the sky data, independent of their great differences. Similarly, the next 4 runs have C band rates of about 60 per second, similar to the minimum sky rates, and independent of their differences. We have seen that these C band rates can be reasonably predicted by combining equations (58) and (61). For coulomb heating models which have not yet equilibrated their electron and ion temperatures, the resulting predicted carbon band rate can be written

$$C \sim 116 \left(\frac{n_o}{0.004\ cm^{-3}}\right)^{7/5} \left(\frac{T_s}{10^6\ K}\right)^{1/10} \left(\frac{E_o}{5 \times 10^{50}\ ergs}\right)^{1/5} \qquad (62)$$

where the Sedov solution ($P_o = 0$) was assumed to remove the dependence on t and R , and T_e' was taken as the plateau value of equation (39). Similarly, for $T_e \simeq T_i$, the carbon band rate is approximately

$$C \sim 86 \left(\frac{n_o}{0.004\ cm^{-3}}\right)^{4/3} \left(\frac{T_s}{10^6\ K}\right)^{1/3} \left(\frac{E_o}{5 \times 10^{50}\ ergs}\right)^{1/6} . \qquad (63)$$

From these two equations, the insensitivity of the carbon band rate to all parameters other than density is apparent, so long as $T_s \sim 10^6$ K is chosen as a prerequisite for fitting the spectrum, and p_o is not too large. Thus the models confirm the equilibrium-calculated estimate that $n_o \sim 0.004\ cm^{-3}$ is required of any model which attempts to reproduce the background surface brightness. We find here, however, that this is essentially independent of the radius of the blast wave disturbance, particularly for models with only coulomb heating of electrons.

In making a detailed comparison with the observational data, it is necessary to consider the potential contribution from an extrapolation of the extragalactic component which dominates at higher photon energies. A power law extrapolation to low energies, assuming an intervening $N_H = 4 \times 10^{20}$ cm^{-2} as typical, would contribute about 1 count per second in the B band, 7 counts per second in the C band, and 21 counts per second to the M band. Only the M band is altered appreciably and even there, most of the rate remains unexplained. The alterations which these contributions make in the band ratios are shown as B'/C' and M'/C' in Table 3.

The observed B/C ratios range between 0.16 and 0.5, with 0.28 to 0.42 being most common at low intensities (100 counts per second in C band) and 0.22 to 0.39 most common at higher intensities (200 counts per second in C band). Since the models have essentially this same range, the B/C ratio is only a weak discriminant for conditions in the blast wave. It is clear, however, from run 31E that unacceptably high B/C ratios result from low T_e' and low T_o. The ratio is expected to rise rapidly for $T_e' < 10^6$ K, excluding these low temperatures from consideration. Conversely, a very low B/C ratio was achieved only by having $T_e' > 2 \times 10^6$ K, $T_e \approx T_i$ and progress toward ionization equilibrium. The latter condition, however, would require a density considerably higher than allowed by the overall surface brightness.

In short, the observed B/C ratio is consistent with those models with the correct C band rate so long as T_e' lies in the range 1.3 to 2.5 $\times 10^6$ K, whether or not the electrons have equilibrated with the ions, and this consistancy extends to even higher values of T_e' if the electrons are heated only by coulomb collisions.

Finally, none of the models produce M band photons at a rate even close to what is observed on the sky. The simplest interpretation of this (other than that the models are wrong or inappropriate) is that the M band derives primarily from more distant regions, perhaps the galactic corona as mentioned previously. There is, however, an alternative explanation lurking in the results. We have seen that high production of M band requires both high temperature and approach to ionization equilibration, which in turn requires great age at the densities consistent with the C band rate. High temperatures and great age, however, are inconsistent with the models with $R_s \sim 100$ pc since the age is roughly 0.4 R_s divided by the sound speed.

On the other hand, both Loop I and the Barnard's Loop through Eridanus region mentioned previously appear significantly enhanced in M band, and both have been interpreted as the supernova reheating of a previously existing cavity. This interpretation depends in part on the apparent enclosure of these regions by HI shells which would not have been generated by the inferred supernova explosions at their observed states of evolution. Two points follow immediately: 1) although none of the models run here have produced a significant amount of M band, there appear to be similar regions in the sky that do (so that we dare not assert that the background M band rate surely comes from more distant emission); and 2) the existence of a massive HI shell around a region allows confinement of the explosion to a finite region, possibly increasing the age enough that ionization equilibration is approached more fully. This possibility could be explored quantitatively by following the evolution of a blast wave into a region with a steep gradient in ambient density. We have applied the techniques of §I and §II

of this paper to this problem, but have not yet calculated the spectra of such regions. Since M band is preferentially produced in hotter regions, it may be necessary to include thermal conduction and evaporation into the interior in order to suitably model this component.

C. The OVI Column Densities

The OVI absorption measurements discussed by Jenkins (1978a,b) serve as indicators of the general interstellar environment as well as a constraint on the solar environment. With regard to the former, it is possible that O^{+5} generated by the blast waves in a very diffuse interstellar environment produces much of the observed absorption (e.g. McKee and Ostriker, 1977). We focus here however on the local constraint, noting that several stars with distances of order 100 to 500 pc have $N(OVI) \leq 1.3 \times 10^{13}$ cm^{-2}, implying that any blast wave with $R_s \sim$ 100 pc in which the sun finds itself immersed can have N(OVI) no greater than about 10^{13} cm^{-2}.

All but two of the runs performed have N(OVI) between 0.18 and 0.86 $\times 10^{13}$ cm^{-2} in apparent consistency with this constraint (see Table 2). This agreement, however, was achieved by foresight. In all of these nine runs, the external ambient temperature was so high that O^{+6} was the dominant ionization stage before the shock even reached the material. Both runs with low values of T_0 had $N(OVI) \sim 4 \times 10^{13}$ cm^{-2}, distinctly at odds with the constraint.

These machine results can be easily understood. The O^{+5} ionization coefficient between 1 and 3×10^6 K is roughly 10^{-10} $(T/10^6\ K)$ cm^2 s^{-1} (Summers, 1974). Thus an oxygen ion which suddenly finds itself in a high temperature region (temperature T_s for $T_e = T_i$ cases) in which the

electron density is $n_e \sim 4n_o$ will successively proceed through its various stages of ionization, spending a time

$$t(O^{+5}) = \frac{1}{\langle \sigma_I v \rangle n_e} \sim \frac{10^{10}\ cm^{-3}}{4n_o} \left(\frac{10^6\ K}{T_s}\right)\ s \qquad (64)$$

as O^{+5}. If this heating is caused by a strong shockwave moving with speed v_s, then the number of oxygen ions (with abundance A(O) relative to hydrogen) swept in per cm^2 s is A (O) $n_o v_s$, a fraction $f(\leq +5)$ of which are initially in the +5 or lower stages of ionization. The steady state column density of O^{+5} ions behind the front is thus $f\ (\leq +5)\ A(O)\ n_o v_s\ t(O^{+5})$. For $A(O) \sim 7 \times 10^{-4}$, and $v_s \sim 3 \times 10^7\ (T_s/10^6\ K)^{1/2}$ cm s^{-1}, the resulting column density should be

$$N(OVI) \sim 5 \times 10^{13} \left(\frac{10^6}{T_s}\right)^{1/2} f(\leq +5)\ cm^{-2}, \qquad (65)$$

independent of n_o and the shock radius, and roughly in accord with the machine results, particularly for the $T_e = T_i$ cases. The dependence on $f(\leq +5)$ is confirmed since for 21E and 31E, f = 1 whereas for all others except 41E, f = 0.1. For 41E, $T_o = 10^6$ K, f is even smaller and N(OVI) has its lowest value. In addition, the weak increase of column density with decreasing T_s is apparent, as is about a factor of 2 higher N(OVI) for all $T_e < T_i$ cases. The latter is due to having a lower ionizaton coefficient in these runs than is appropriate for T_s. Finally we note that in all cases the column densities are significantly in excess of the equilibrium values, the excess decreasing with time.

The consequences for the models are rather harsh. In order to hold the OVI column density to an acceptable level, one of the following seems

to be required:

a) The oxygen abundance is about a factor of four lower than stated;

b) T_0 is sufficiently high that most of the oxygen is in the +6 stage;

c) The ambient oxygen is found mostly in the +6 stage from past history even though T_0 is now low;

d) The post-shock temperature must be significantly higher to raise the O^{+5} ionization coefficient (which, however, has a maximum of only 8 x $10^{-10} cm^2\ s^{-1}$ at $T \sim 10^7$ K);

e) The O^{+5} ions experience considerable photoionization;

f) The rate of incorporation of new material proceeds at considerably less than the sound speed for the temperature to which they are heated; or

g) The OVI constraint has been exaggerated.

We have the following comments on these possibilities;

a) The presence of oxygen-bearing dust could contribute to this effect, but the dust would have to survive in the post shock environment.

b) Any temperature greater than about 3×10^5 K is sufficient to make N(OVI) within the shocked region less than $10^{13}\ cm^{-2}$. In this case, however the explosion serves to deplete a region of O^{+5}, not to produce it. Thus there is the additional constraint that if the ambient medium (with density $n_0 = 0.004\ cm^{-3}$) occupies a significant portion of the insterstellar volume, it must have $n(O^{+5}) \leq 2 \times 10^{-8}\ cm^{-3}$. With $A(O) \sim 7 \times 10^{-4}$, this implies that less than 1% of the oxygen is in the +5 stage, requiring $T_0 \geq 8 \times 10^5$ K. At a just slightly higher temperature, the ambient medium becomes a profuse radiator of soft X-rays and we revert to the model of Cox and Smith (1974) with no need for the local explosion.

c) This suggestion seems to be untenable. The radiative recombination timescale of O^{+6} with $n_e \sim 4 \times 10^{-3}$ cm^{-3} and $T_e < 10^6$ K is less than 1.3×10^7 years, but since only 1% can have recombined without violating the constraint on the ambient medium, less than 10^5 years can have elapsed since the temperature fell. This timescale is much shorter than the approximately 10^6 years between strong blast waves in typical regions making recombination hysteresis an unacceptable hypothesis. This could be alleviated somewhat if the oxygen were left in the +7 or +8 stage, but the implied high ionization stages of other elements would probably make production of B band photons difficult when the shock arrived.

d) This may help somewhat in conjuction with either of possibilities f) or g).

e) The photoionization timescale for O^{+5} in the calculated radiation environments is of order 10^{15} seconds, about a factor of 10^{+3} too long to be of significance.

f) This may be possible for models evolving in a pre-existing cavity with a strong density gradient and will be explored in future work.

g) The constraint is only about a factor of four lower than the OVI column densities achieved for the low T_0 models. Since OVI is more difficult to measure for high temperature components which are broader and shallower than those actually seen, high temperature shocks could conceivably give profiles consistent with the measurements.

V. Summary and Conclusions

In setting out to study the possibility that the soft X-ray background might derive from our being located inside a very large-scale blast wave, we soon realized that the external pressure was important to the details because the blast radii were in many cases comparable to the characteristic radius defined by equation (5). In §I, we managed to extend the approximation scheme of Kahn (1975) to find analytical expressions for the evolving dynamics. These descriptions are expected to be reasonably accurate throughout the structure for $y_s > 6$, $R_s < 1.27\ R_c$; and for the bulk of the material, which is located near the outer edge, until at least $y_s \sim 2$, $R_s \sim 2.5\ R_c$.

In §II, we discuss the potential effects of electron heating and thermal conduction, settling on 2 adiabatic models which would reasonably describe most of the possible situations, particularly at late times. We also applied Itoh's (1978) formulation of coulomb heating to find analytic expressions for the electron temperature distribution of the evolving structure. These expressions are valid in detail only if this is the sole mechanism for electron heating and if thermal conduction is negligible. It was shown, however, that with only coulomb collisions heating the electrons, thermal conduction would always be modest. The effects could, however, be just as important at $t \sim t_{eq}$ as are the non-negligible external pressure effects at $R_s \sim R_c$.

We were concerned that the blast waves we were studying might be beyond the point that radiative cooling upsets adiabaticity. Hence we restudied the question of the cooling timescale of a strong blast wave with particular attention to whether the equilibrium cooling coefficient

could reasonably be used in the evaluation. Our conclusion was that it could be used with confidence even though collisional equilibrium of the ions would not always be fully established.

For strong blast waves, we were able to conclude that collision-related phenomena occurred in a fixed sequence: thermal conduction fades in importance just as electrons are heated by coulomb collisions; later the collisional equilibrium cooling coefficient becomes a reasonable approximation, and finally significant cooling takes place. We expect this sequence to remain even when the ambient pressure is not negligible and conclude that we can tell whether radiative cooling is important in cases of interest by observing the location of the results of detailed computer runs within this sequence. None of the cases in this study were found in this way to have left the adiabatic regime.

In §III, we presented the method with which we were able to follow the history of an individual gas parcel through the structure so that the ionization equations could be integrated. We then outlined the computer program which used the methods of these 3 sections to model the blast waves in our study. For a set of diagnostic runs, the luminosity evolution was compared with simple models. It was found that the luminosity could be predicted to within a few percent in many cases; and when the estimates were found to be less accurate, the discrepancies could be rationalized. We presented the detailed structures and spectra of 2 runs to complete the picture before going on to our specific application to the soft X-ray background.

In §IV, we presented the appearance of our diagnostic runs to the Wisconsin soft X-ray rocket payload, as count rates in the B, C, and M bands. For the C band rates, it was found that the rate for a particular

explosion varied very little with time and radius, and that this could be understood from the estimated luminosity evolution. The results for this band (with modest p_0) are summarized in equations (62) for $t < t_{eq}$ and (63) for $t > t_{eq}$ or $T_e \approx T_i$. We conclude immediately that the ambient density must be $n_0 \sim 0.004$ cm^{-3} to give the observed carbon band rate, although an implicit assumption, so that the dominant cooling falls in the C band, was that $T_s \sim 10^6$ K.

Once n_0 has been determined by the C band surface brightness, the B band rate is still available to determine the evolutionary state (T_s, R_s, t) for a given type of model. As it turns out, however, the ratio of B rate to C rate (B/C) is rather insensitive to the desired parameters, since it tends to increase as T_e falls but decrease as the evolution approaches equilibrium. We are, however, encouraged by the fact that most calculated examples have B/C within the observed range. For the value of n_0 determined by the C band rate, it appears to be possible to obtain too low a B band rate, only if electrons are equilibrated with the ion temperature by processes other than coulomb collisions and we look very early (when T_e is high).

In contrast, the M band count rates produced by the models were never as large as the observed rates. We noted, however, that two large emission regions present in the soft X-ray maps, regions which could be more distant examples of such blast waves, are quite bright in M band. Thus, although it is possible simply to assume that for the general background the M band derives from some other source (such as the galactic corona) we would at the same time have to conclude that our bubble differs from the two others observed. In addition, the two others, at least, are not well described by the present models.

Neither of the other two bubbles, however, is expected to be described by the models. Both seem to have external hydrogen shells and have been interpreted as blast waves evolving in pre-existing cavities, probably with strong density gradients. We believe that the presence of such a gradient acts in just such a way that M band enhancement will result and have begun to develop the models to test this hypothesis.

The question still remains, even assuming the success of the next generation of models in producing M-band-sensitive photons, whether the general background derives its M band rate from our local bubble. This question probably assumes its greatest significance when we wonder what fraction of the count rate might be attributable to the galactic corona, and may translate to whether or not we are within a pre-existing cavity and whether the blast wave is interacting with a strong density gradient near the cavity boundary. We have only two comments: First, we may be located in a hole in the HI distribution that extends to about 100 pc or even further in some directions (e.g. Bohlin, Savage, and Drake, 1978). Second, we recall the initial reason for inferring that the local bubble had a radius as great as 100 pc: The observed anticorrelation between the count rates in both B and C bands and the HI column density along the line of sight was most easily interpreted as a displacement effect (Sanders, et al., 1977; Cox, 1977). That is, the hydrogen seemed to be intruding into the emitting volume, lowering the emission measure for soft X-rays. The clear implication, if this interpretation survives, is that the blast wave is indeed interacting with strong density gradients in at least some directions.

No strong conclusions, however, should be drawn from these comments. Although we seem to be in a cavity and our local bubble seems to be interacting

with the walls, it is the B and C band rates which vary with this interaction. The M band rate is much more smoothly distributed. On the other hand, the M band rate is also distributed more smoothly than the C band rate within Loop I (McCammon, et al. 1980).

A related problem not addressed by these models is whether the presence of HI regions intruding into the boundary of the blast wave will in fact lower the B and C band rates, as desired, without seriously altering their ratio.

Finally, we addressed a constraint placed on the blast wave (and the ambient medium into which it propagates) by OVI column density measurements. We found that for blast waves propagating into homogeneous cold material, the OVI column densities exceeded the local constraint by a factor of about four. This could be remedied by having the ambient medium already highly ionized (mostly as O^{+6}), but then the ambient medium, alone, contained too much O^{+5} unless the ambient temperature exceeded 8×10^6 K. With an ambient temperature just slightly higher than this lower limit, the blast wave is not needed to produce the X-rays and we revert to the initial model of Cox and Smith (1974).

Other schemes for lowering the OVI column density were also discussed along with the possibility that the constraint was exaggerated. Two hopeful possibilities are related to the concept of there being a pre-existing cavity: for evolution in a strong density gradient, the OVI column density may be reduced to an acceptable level even for $T_0 = 0$; and, quite possibly, the "ambient medium" should not be thought of as extending throughout a large portion of the interstellar volume. It may, instead, be localized within large but discrete

cavities, most of which have been reheated sufficiently recently that little O^{+5} is present except at the boundaries.

Finally, we reiterate our successes: we have managed to model a blast wave in a homogeneous region of finite pressure, and to show that if the solar system were located within such a blast wave with $n_0 \sim 0.004$ cm^{-3}, $E_0 \sim 5 \times 10^{50}$ ergs, and $R_s \sim 100$ pc, the Wisconsin soft X-ray rocket payload would measure the B and C band count rates which it does. The explosion age would be just over 10^5 years.

This research was supported, in part, by NASA grant NGL 50-002-044 at the University of Wisconsin. The paper was written largely while Don Cox was a Visiting Associate Professor in the Department of Space Physics and Astronomy at Rice University and he wishes to extend his gratitude for their support and encouragement. We both wish to thank Wilt Sanders for his immeasurable help at all the right times and to acknowledge useful conversations with, and invaluable computer programs of John Raymond, along with the generally stimulating and helpful environment of the Space Physics Group at Wisconsin. John Nousek and Dave Burrows were of particular assistance.

TABLE LUMINOSITY EVOLUTION

GROUP A: EVOLUTION IN TIME

$E_o = 5 \times 10^{50}$ ergs, $n_o = 5 \times 10^{-3}$ cm^{-3}, $T_o = 5 \times 10^5$K, $R_c = 86.0$ pc,

$t_{eq} = 3 \times 10^{12}$s, $t_E = 4 \times 10^{12}$s, $t_1 = 1.7 \times 10^{13}$s

Electrons heated only by coulomb collisions with ions

RUN #	R_s (pc)	t (10^{12}s)	T_{s_6} (10^6K)	T_e(max) (10^6K)	$\mathcal{L}$,(approx)[b] (10^{35}erg s^{-1})		$\mathcal{L}_{CE}$,(approx)[c] (10^{35}erg s^{-1})	
3E	55.7	1.20	4.82	2.9[a]	2.97	(3.4)	1.19	(.84)
2E	71.3	2.20	2.64[a]	2.7	5.27	(5.3)	2.61	(1.8)
1E	83.7	3.18	1.54[a]	2.4	6.69	(6.2)	4.40	(3.9)
4E	102	5.09	1.34[a]	2.6[e]	10.[illegible]	(8.6)[g]	7.46	(7.6)[g]
	Similar but with $T_e = T_1 = T$							
2	71.3	2.20	2.64[a]	———	5.54	(5.3)	1.67	(1.8)
1	83.7	3.18	1.54[a]	———	6.74	(6.2)	4.04	(3.9)

GROUP B: DEPENDENCE ON T_o

$E_o = 5 \times 10^{50}$ ergs, $n_o = 2.7 \times 10^{-3}$ cm^{-3}, $R_s = 102$ pc,

$t_{eq} = 4 \times 10^{12}$s, $t_E = 6 \times 10^{12}$s, $t_1 = 2.4 \times 10^{13}$s

RUN #	R_c (pc)	T_o (K)	t (10^{12}s)	T_{s_6} (10^6K)	T_e(max) (10^6K)	$\mathcal{L}$,(approx)[b] (10^{35}erg s^{-1})		$\mathcal{L}_{CE}$,(approx)[c] (10^{35}erg s^{-1})	
31E	581	3×10^3	4.02	1.27[a]	2.2[e]	33.3[d]	(3.8)	2.86	(2.3)
11E	106	5×10^5	3.85	1.93[a]	2.3	3.97	(4.3)	2.28	(1.8)
41E	83.8	1×10^6	3.72	2.57	2.4[a]	2.87[h]	(4.7)	2.00	(1.6)
	above: electrons heated only by coulomb collisions								
	below: $T_e = T_1 = T$								
11	106	5×10^5	3.85	1.93[a]	———	4.21	(4.3)	1.93	(1.8)

GROUP C: A DENSER EXAMPLE

$E_o = 5 \times 10^{50}$ ergs, $n_o = 0.16$ cm^{-3}, $T_o = 1 \times 10^4$K, $R_c = 99.8$ pc,

$t_{eq} = 0.4 \times 10^{12}$s, $t_E = 0.6 \times 10^{12}$s, $t_1 = 2.1 \times 10^{12}$s

RUN #	R_s (pc)	t (10^{12}s)	T_{s_6} (10^6K)	T_e(max) (10^6K)	$\mathcal{L}$,(approx)[b] (10^{35}erg s^{-1})		$\mathcal{L}_{CE}$,(approx)[c] (10^{35}erg s^{-1})	
21E	21	0.60[c]	2.41[a]	6.5[e]	179[f]	(53)[f]	54.4	(51)[f]

Footnotes to Table 1

a) Electron temperature used in estimating luminosities

b) From equation (58)

c) From equation (59)

d) A substantial contribution, (29.0×10^{35} erg s^{-1}, versus 0.6×10^{35} erg s^{-1} for run 11E, with $h\nu < 55$eV) arises from low stages of ionization which the program does not resolve well. The X-ray and EUV luminosity is better represented by the approximate results.

e) The plateau temperature is not well defined for $t > t_{eq}$. T_e is still rising inward of our last zone.

f) Example for which $t = t_E$.

g) Although nominally, $t > t_E$, the external pressure has lowered the compaction parameter so that α_{CE} is over estimated. In addition, incomplete ionization of the carbon K shell enhances the nonequilibrium rate somewhat, delaying its approach to the equilibrium value.

h) For large T_0, two effects depress the cooling rate below the estimated result. One is the lower post shock compression factor; the other is the high preionization, resulting in higher (and less emissive) stages of ionization in the cooling region.

i) As in run 31E, the total luminosity includes large, possibly erroneous contributions at low photon energies (106×10^{35} erg s^{-1} for $5\text{eV} < h\nu < 55\text{eV}$ and 19×10^{35} erg s^{-1} for $55\text{eV} < h\nu < 105\text{eV}$) because the low T_0 allows low transient stages of ionization just inside the shock.

TABLE 2. BAND RATES AND N(OVI)

RUN #	T_e' (10^6K)	n_o (cm^{-3})	R_s (pc)	B (s^{-1})	B_{CE}	C (s^{-1})	C_{CE}	M (s^{-1})	M_{CE}	N(OVI), (CE) ($10^{13}cm^{-2}$)
3E	2.9	$5.0x10^{-3}$	55.7	62	13	154	68	9	5	.71 (.06)
2E	2.64	"	71.3	66	22	170	100	8	5	.68 (.10)
1E	1.54	"	83.7	65	40	142	120	3	3	.86 (.24)
4E	1.34	"	102	70	53	155	140	3	3	.83 (.27)
2	2.64	"	71.3	49	5	176	41	23	11	.35 (.02)
1	1.54	"	83.7	61	31	161	128	6	5	.56 (.14)
31E	1.27	$2.7x10^{-3}$	102	27	17	50	46	1	1	4.73 (.17)
11E	1.93	"	102	26	13	57	45	1	1	.67 (.13)
41E	2.5	"	102	23	10	62	43	2	2	.18 (.10)
11	1.93	"	102	24	6	70	37	5	3	.38 (.05)
21E	2.41	0.16	21.1	6,140	2,550	29,400	17,500	5,470	3,210	3.99 (.25)

Table 3

RATIOS OF BAND COUNT RATES

RUN #	T'_e (10^6K)	B/C	M/C	B'/C'	M'/C'
3E	2.9	0.40	0 06	0.39	0.19
2E	2.6	0.39	0.04	0.38	0.16
1E	1.5	0.46	0.02	0.44	0.16
4E	1.3	0.45	0.02	0.44	0.15
2	2.6	0.28	0.13	0.27	0.24
1	1.5	0.38	0.04	0.37	0.16
31E	1.3	0.54	0.02	0.48	0.39
11E	1.9	0.46	0.03	0.42	0.35
41E	2.6	0.37	0.03	0.34	0.33
11	1.9	0.34	0.07	0.32	0.33
21E	2.4	0.21	0.19	0.21	0.19

Primed ratios include 1 cps in B band, 7 cps in C band, and 21 cps in M band as typical contribution of extrapolated and absorbed high energy extragalactic power law.

REFERENCES

Bohlin, R. C., Savage, B. D. and Drake, J. F. 1978, Ap.J., 224, 132

Borken, R. J. and Iwan, D. C. 1977, Ap. J., 218, 511.

Burstein, P., Borken, R. J., Kraushaar, W. L., and Sanders, W. T. 1976, Ap. J., 213, 405.

Chevalier, R. A. 1974, Ap. J., 188, 501.

Chevalier, R. A. 1975, Ap. J., 198, 355.

Chevalier, R. A. 1977, Ann. Rev. Astron. Astrophys., 15, 175.

Cowie, L. L. 1977, Ap. J., 215, 226.

Cowie, L. L. and McKee, C. F. 1977, Ap. J., 211, 135.

Cox, D. P. 1972, Ap. J., 178, 143.

Cox, D. P. 1977, Topics in Interstellar Matter, ed. H. van Woerden, (Dordrecht and Boston: Reidel) p. 17.

Cox, D. P. and Franco, J. 1981, submitted to Ap.J.

Cox, D. P. and Smith, B. W. 1974, Ap. J. (Letters), 189, L105.

Cox, D. P. and Tucker, W. H. 1969, Ap. J., 157, 1157.

Fried, P. M., Nousek, J. A., Sanders, W. T., and Kraushaar, W. L. 1980, Ap.J., 242, 787.

Gaffet, B. 1978, Ap.J., 225, 442.

Gronenschild, E. H. B. M. and Mewe, R. 1979, Chapter VI Gronenschild's thesis, Utrecht.

Itoh, H. 1978, Publ. Astr. Soc. Japan, 30, 489.

Itoh, H. 1979, Publ. Astr. Soc. Japan, 31, 541.

Jenkins, E. B. 1978, Ap. J., 219, 845.

Jenkins, E. B. 1978, Ap. J., 220, 107.

Jones, E. M. 1978, private communication.

Kahn, F. D. 1975, Proceedings of 14th Intl. Cosmic Ray Conf., Munich, Germany, 11, 3566.

Kahn, F. D. 1976, Astr. Ap., 50, 145.

Kraushaar, W. L. 1979, (COSPAR) X-Ray Astronomy, eds. W. A. Baity and L. E. Peterson (Oxford and New York: Pergamon), p. 293.

McCammon, D. 1980, Kraushaar, W. L., Sanders, W. T., and Burrows, D. N., 1980, Proceedings of 16th Intl. Cosmic Ray Conf., Kyoto, Japan.

McKee, C. F. and Hollenbach, D. J. 1980, Ann. Rev. Astron. Astrophys., 18, 219.

McKee, C. F., and Ostriker, J. P. 1977, Ap. J., 218, 148.

Nousek, J. A., Fried, P. M., Sanders, W. T., and Kraushaar, W. L. 1981, in preparation.

Raymond, J. C., Cox, D. P., and Smith, B. W. 1976, Ap. J., 204, 290.

Raymond, J. C. and Smith, B. W. 1977, Ap. J. Suppl., 35, 419.

Reynolds, R. J. and Ogden, P. M. 1979, Ap. J., 229, 942.

Sanders, W. T., Kraushaar, W. L., Nousek, J. A., and Fried, P. M. 1977, Ap. J., 217, L87.

Sedov, L. I. 1959, Similarity and Dimensional Methods in Mechanics (New York: Academic Press).

Shklovsky, I. S. 1968, Supernovae (New York: Interscience).

Solinger, A., Rappaport, S., and Buff, J. 1975, Ap. J., 201, 381.

Spitzer, L. 1962, Physics of Fully Ionized Gases (New York: Wiley Interscience).

Summers, H. P. 1974, I. M. 367, Appleton Laboratory, Culham Laboratory, Ditton Park, Slough, England.

Taylor, G. I. 1950, Proc. Roy. Soc. London, A, 101, 159.

FIGURE CAPTIONS

Figure 1. End result of adiabatic blast wave. Final density distribution, $x_f = n_f/n_o$, and mass expelled from within R.

Figure 2. Dynamical and thermal structures of runs 11 and 11E. a) pressure; b) density; c) temperature, solid line is mean temperature for both and electron temperature for run 11, whereas dashed line is electron temperature for run 11E.

Figure 3. Distribution of ionization stages of oxygen. a) run 11, b) run 11E.

Figure 4. Surface brightness spectra in 5eV bins. Unit is 10^{-23}erg cm^{-2} s^{-1} sr^{-1} per bin. a) run 11, b) run 11 with collisional equilibrium ion concentrations, c) run 11E, d) run 11E with collisional equilibrium ion concentrations.

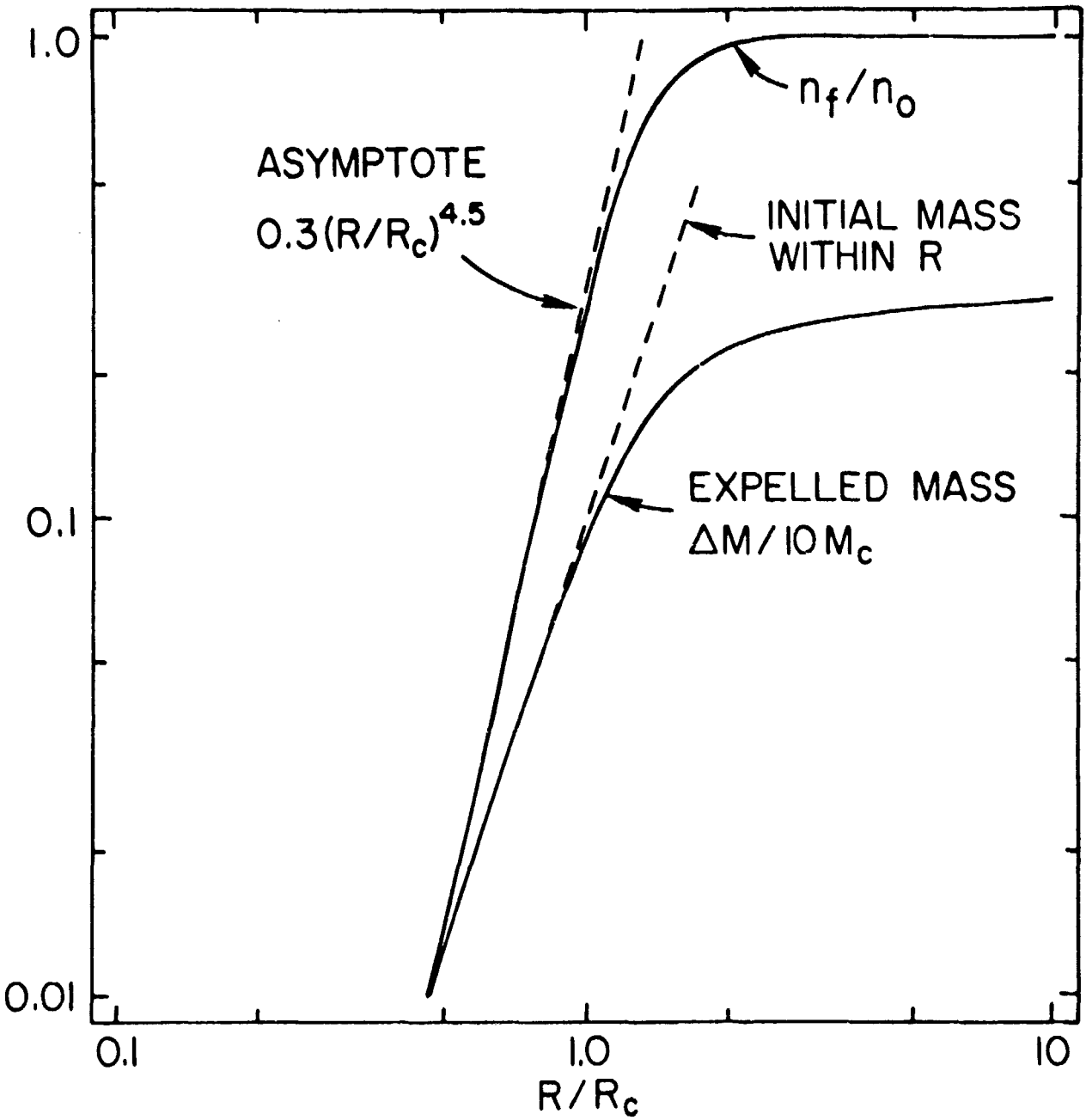
1.0
0.1
0.01
0.1
1.0
10
R/Rc
nf/no
ASYMPTOTE
0.3(R/Rc)4.5
INITIAL MASS
WITHIN R
EXPELLED MASS
ΔM/10Mc

Figure 1

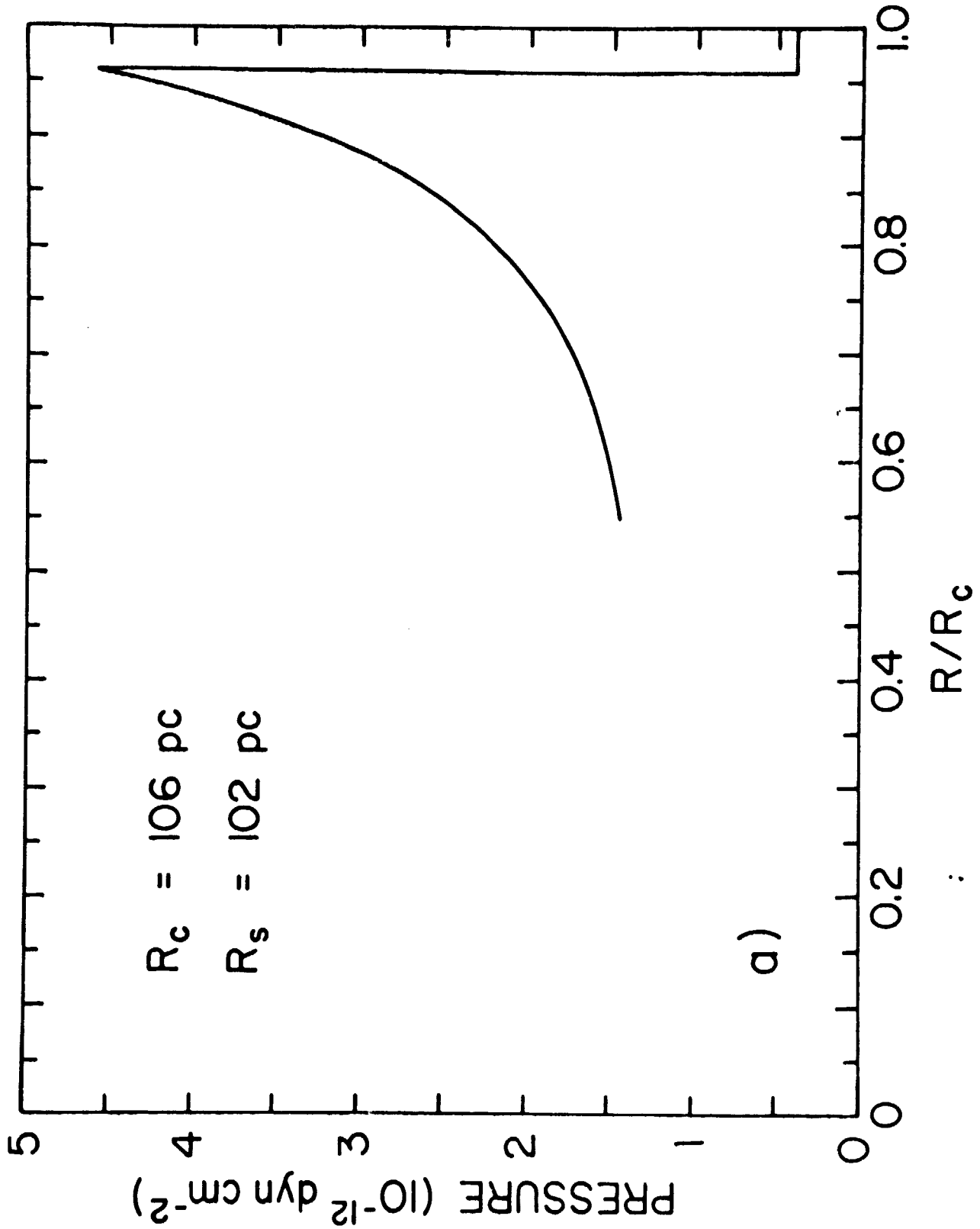
PRESSURE (10⁻¹² dyn cm⁻²)
0
1
2
3
4
5
0
0.2
0.4
0.6
0.8
1.0
R/Rc
Rc = 106 pc
Rs = 102 pc
a)

Figure 2a

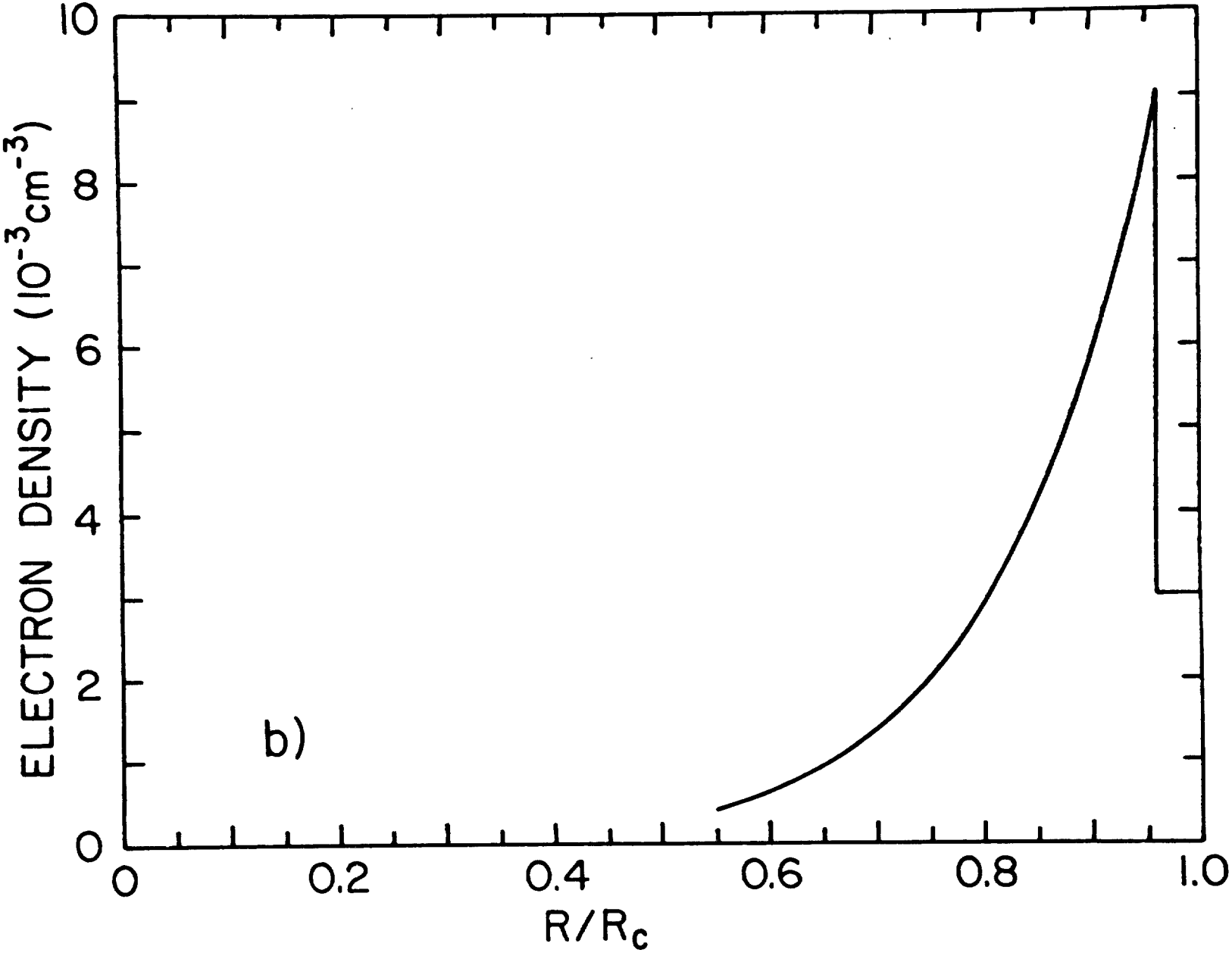

Figure 2b

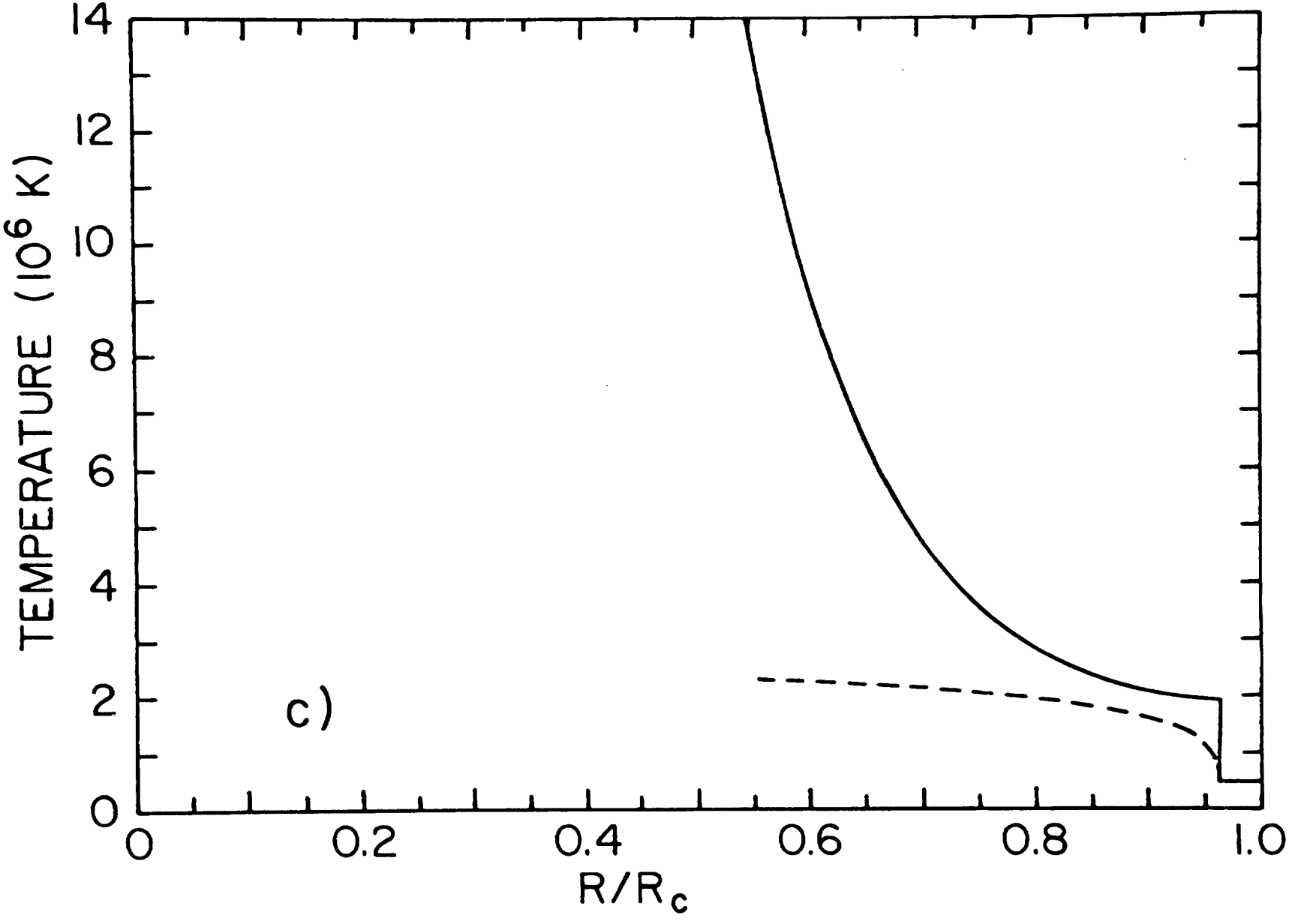

Figure 2c

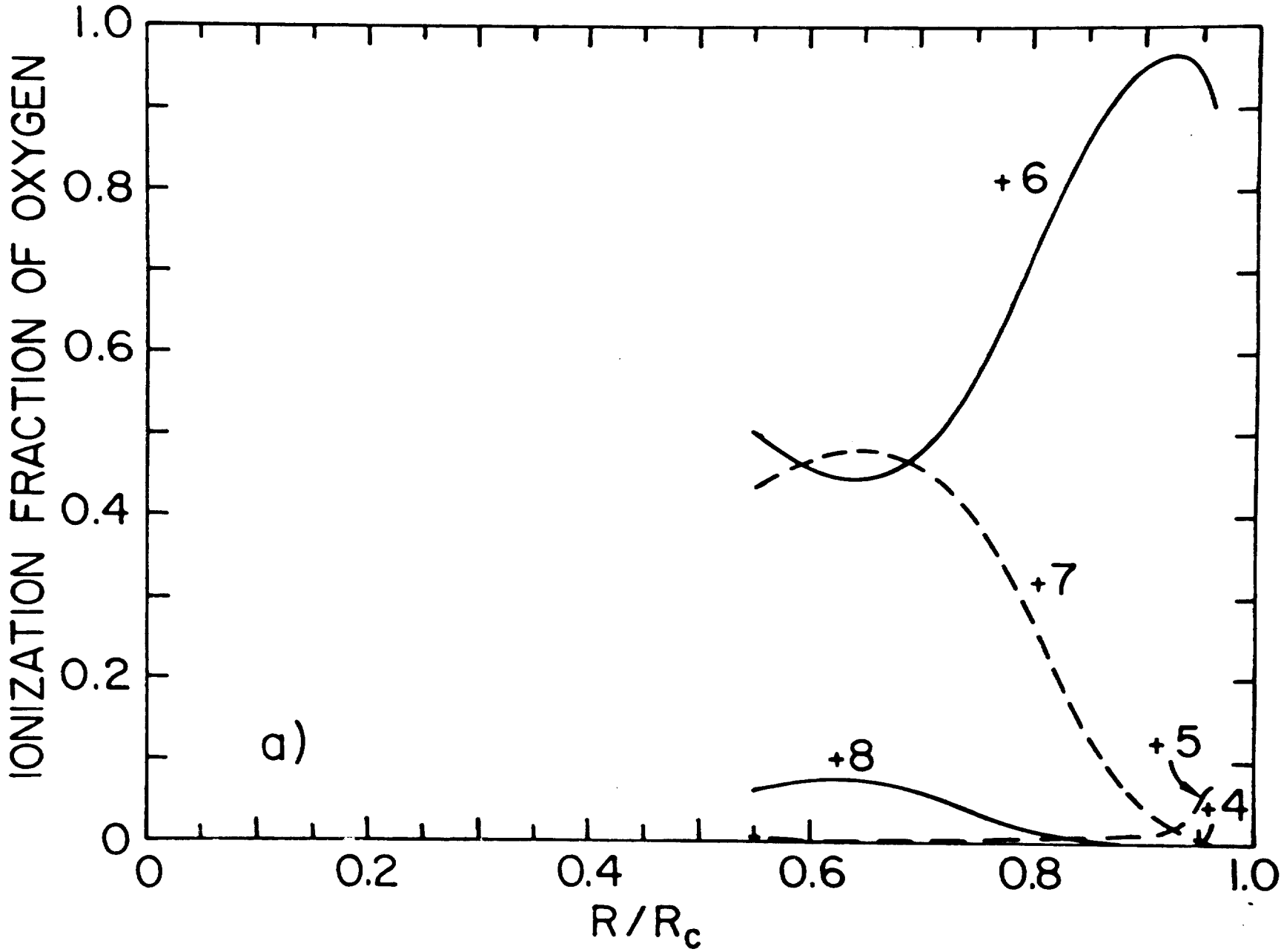
IONIZATION FRACTION OF OXYGEN
1.0
0.8
0.6
0.4
0.2
0
0
0.2
0.4
0.6
0.8
1.0
R/Rc
a)
+6
+7
+8
+5
+4

Figure 3a

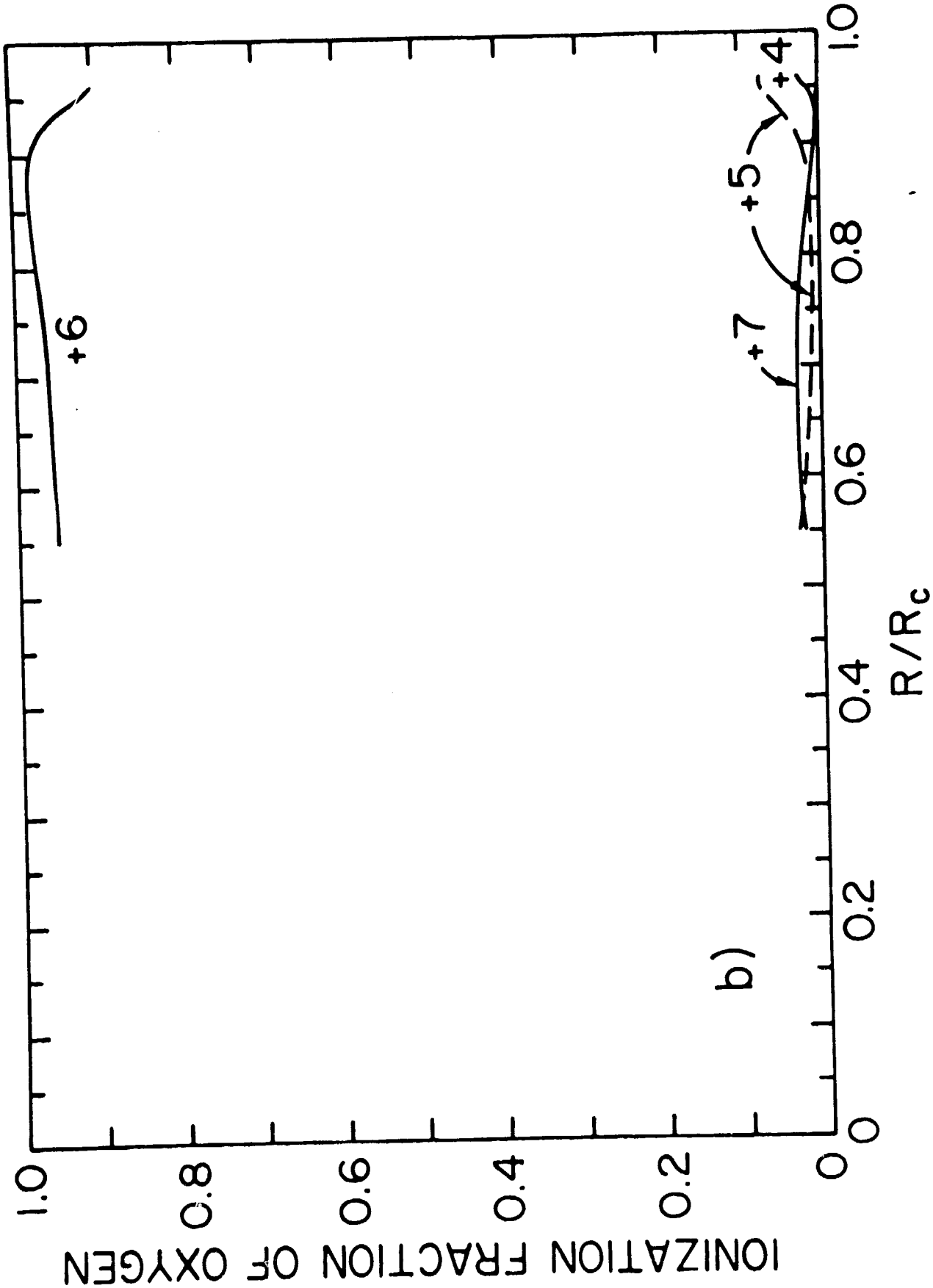
IONIZATION FRACTION OF OXYGEN
1.0
0.8
0.6
0.4
0.2
0
0
0.2
0.4
0.6
0.8
1.0
R/Rc
b)
+4
+5
+7
+6

Figure 3b

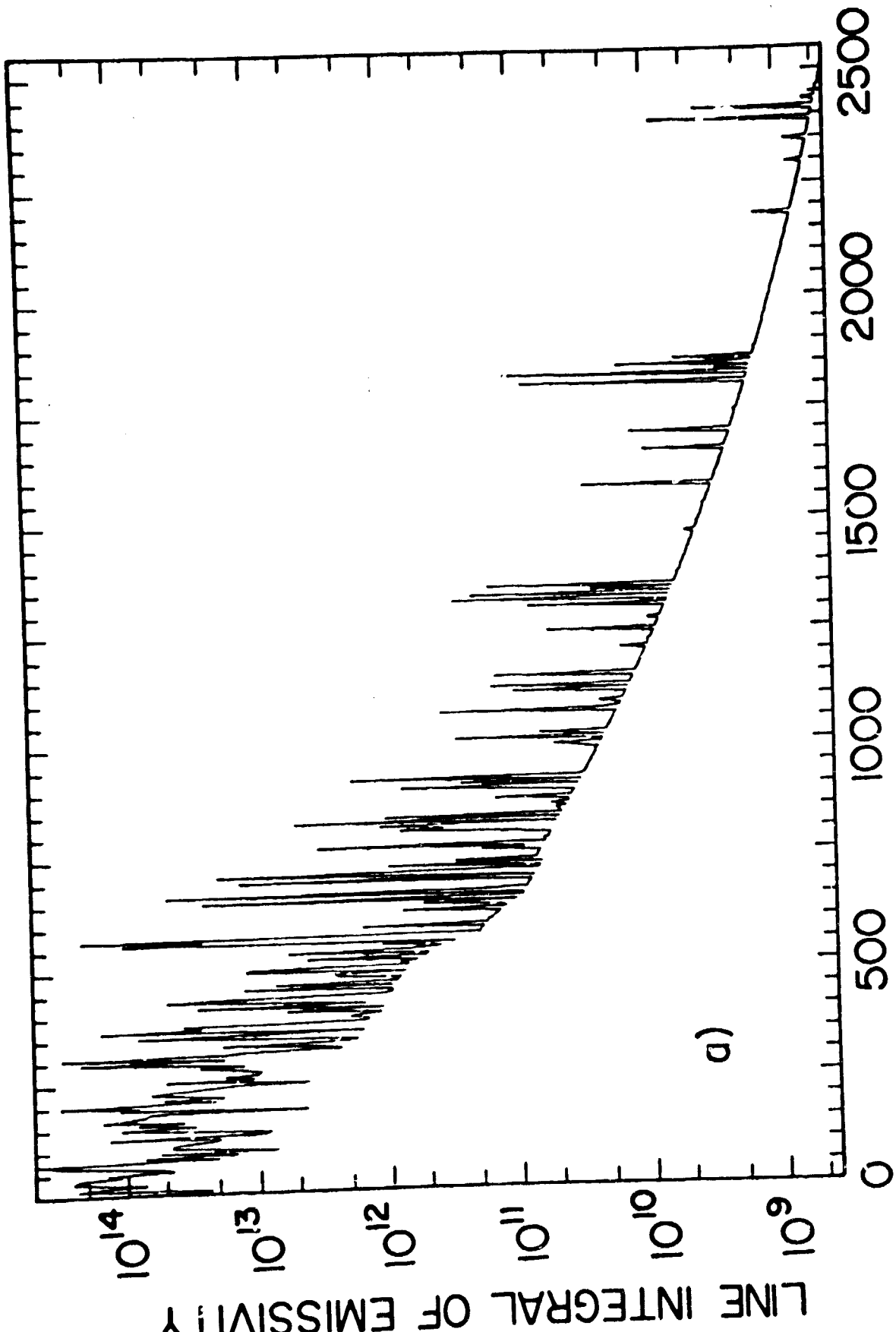
LINE INTEGRAL OF EMISSIVITY
10^{14}
10^{13}
10^{12}
10^{11}
10^{10}
10^{9}
0
500
1000
1500
2000
2500
ENERGY (eV)
a)

Figure 4a

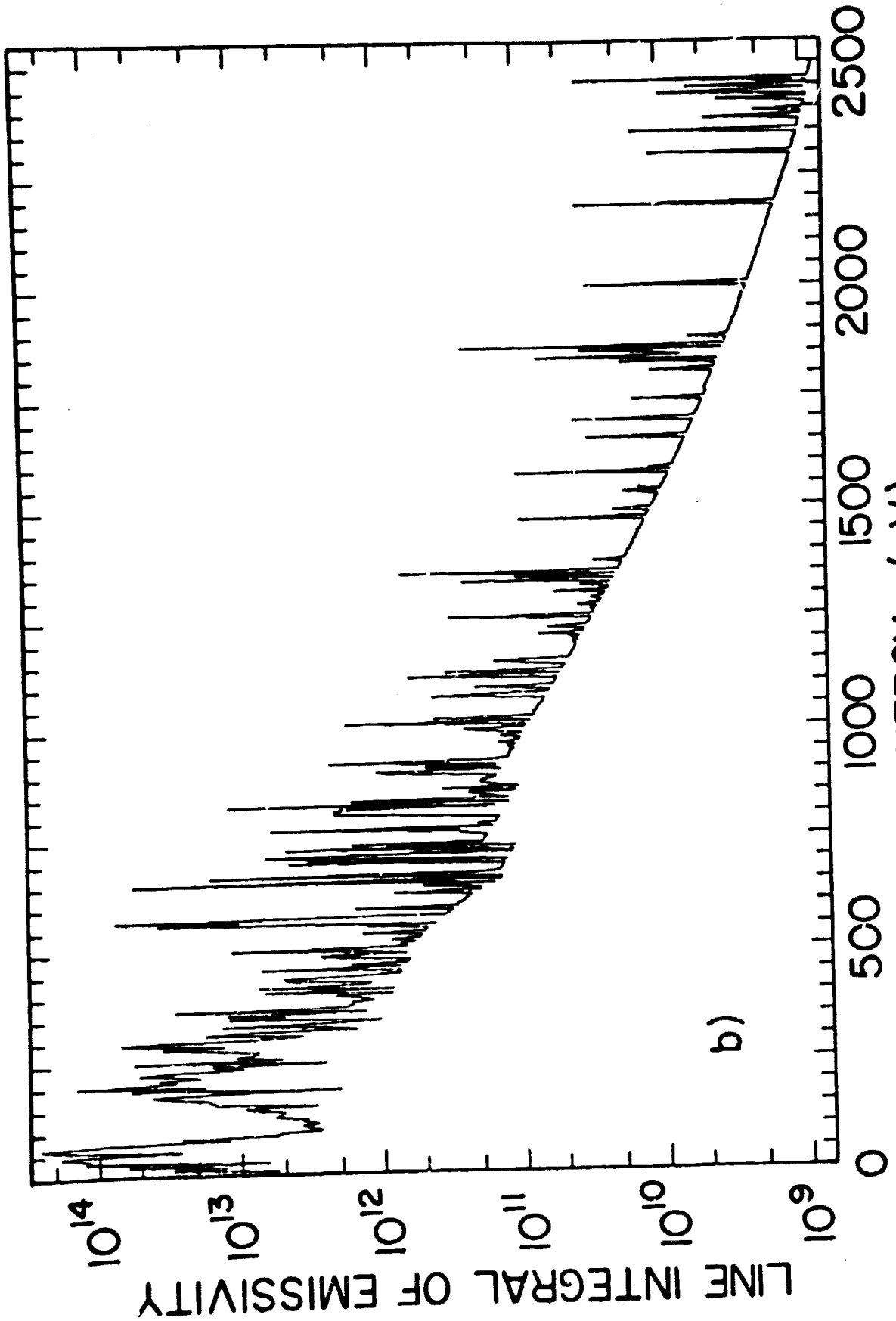
LINE INTEGRAL OF EMISSIVITY
10^{14}
10^{13}
10^{12}
10^{11}
10^{10}
10^{9}
0
500
1000
1500
2000
2500
ENERGY (eV)
b)

Figure 4b

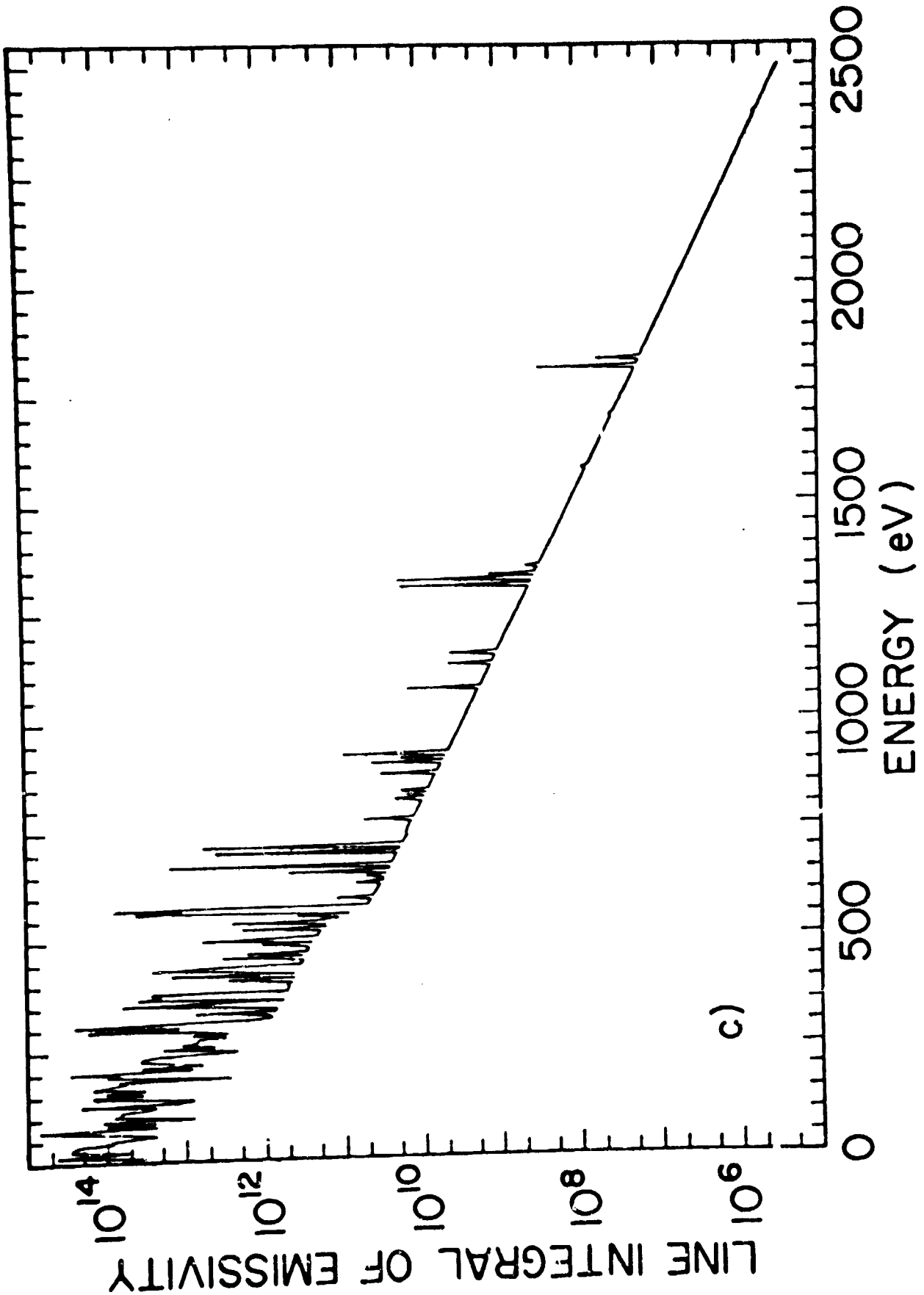
LINE INTEGRAL OF EMISSIVITY
10^{14}
10^{12}
10^{10}
10^{8}
10^{6}
0
500
1000
1500
2000
2500
ENERGY (eV)
c)

Figure 4c

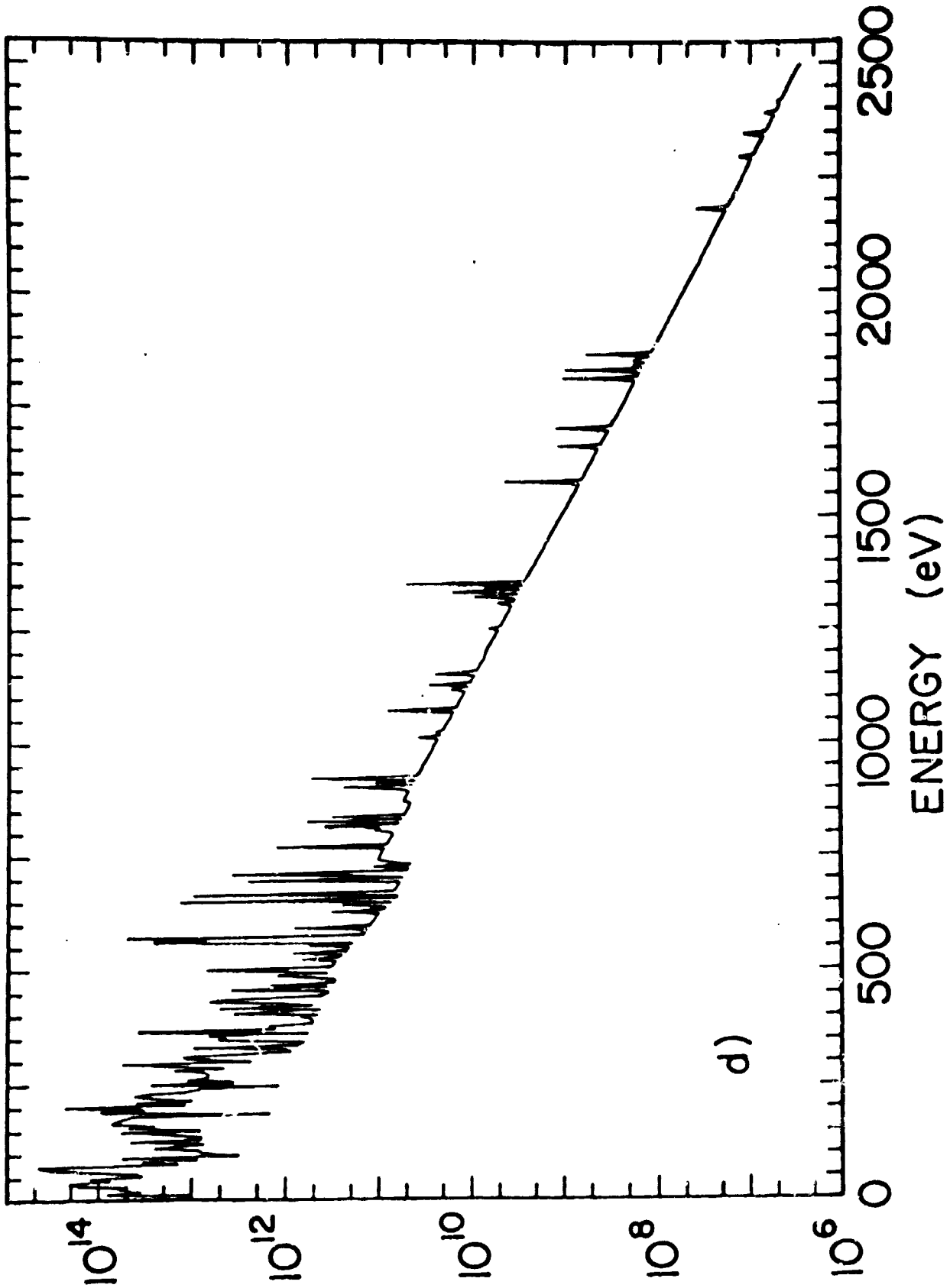
LINE INTEGRAL OF EMISSIVITY
10^{14}
10^{12}
10^{10}
10^{8}
10^{6}
0
500
1000
1500
2000
2500
ENERGY (eV)
d)

Figure 4d

Donald P. Cox: Department of Physics, University of Wisconsin,
1150 University Avenue, Madison, Wisconsin 53706.

Paul R. Anderson: Physics Department, University of California,
Santa Barbara, California 93106.